doi:10.1038/nature11923

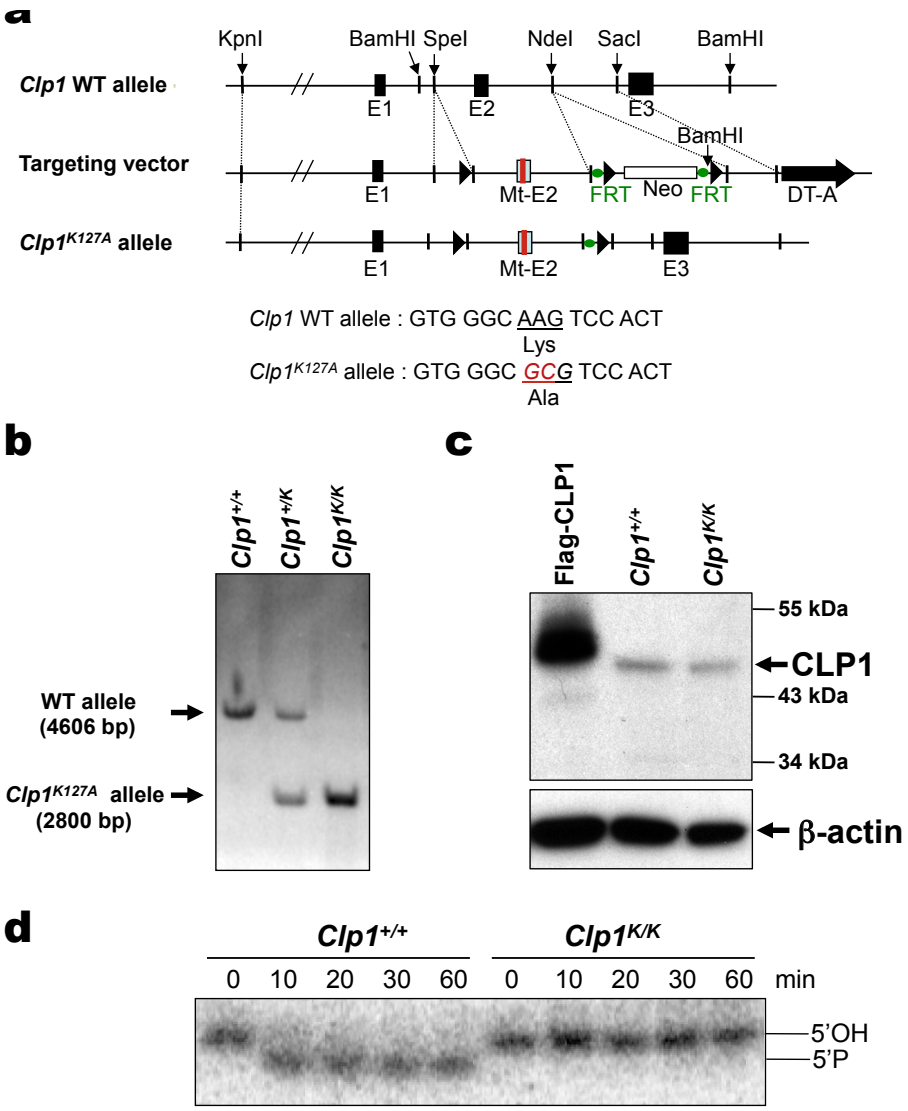

Supplementary Figure 1. Generation of *Clp1* kinase-dead knock-in mice.

a, Targeting strategy to generate *Clp1* kinase-dead knock-in mice. The genomic structure of the wild type murine *Clp1* gene, the targeting vector and the targeted alleles are indicated. The $Clp1^{K127A}$ mutation was generated by PCR site-directed mutagenesis. The mutant exon 2 (Mt-E2) is flanked by *LoxP* sequences (black triangles). The Neo cassette is flanked by *frt* sites (green circles). The modified *Clp1* gene locus after excision of the Neo cassette following transient expression of Flp recombinase ($Clp1^{K127A}$ allele) is shown. **b,** Southern blot analysis of BamHI digested genomic DNA from F2 wild type (WT), heterozygous $Clp1^{K/+}$ and homozygous mutant $Clp1^{K/K}$ littermates obtained from intercrosses between F1 heterozygous mice. The wild type (WT) and mutant $Clp1^{K127A}$ alleles are indicated. **c,** Western blot analysis of protein extracts from MEFs confirmed apparently normal CLP1 protein expression in $Clp1^{K/K}$ mice. Lysates from HEK293T cells overexpressing Flag-tagged CLP1 were used as a positive control. β-actin is shown as a loading control. **d,** RNA kinase activity assay of protein extracts from $Clp1^{+/+}$ and $Clp1^{K/K}$ MEFs. Cell lysates were incubated with an RNA duplex bearing a 5'-OH group and [^{32}P]Cp 3' end-label at one strand for the indicated time points. RNA phosphorylation results in a migration shift after running the reaction products in a denaturing acrylamide gel.

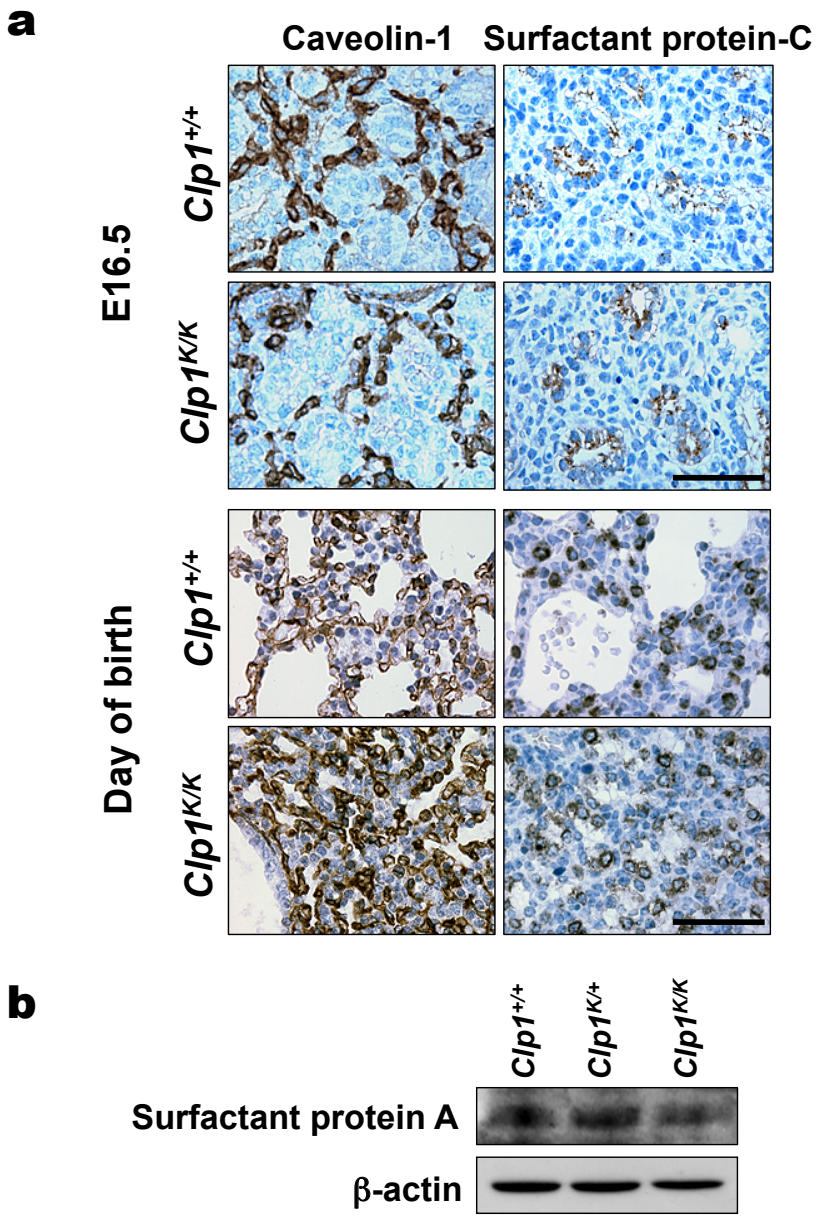

Supplementary Figure 2. Normal lung development in *Clp1*$^{K/K}$ mice.

a, Immunostaining of lungs from embryonic day 16.5 (E16.5) and neonatal *Clp1*$^{+/+}$ and *Clp1*$^{K/K}$ littermates using prototypic type I (Caveolin-1) and type II (Surfactant protein C) pneumocyte markers. Scale bars: 50 μm. **b,** Western blot analysis of E18.5 lung tissue lysates confirms intact pulmonary surfactant protein A expression in *Clp1*$^{K/K}$ mice. β-actin is shown as a loading control.

a

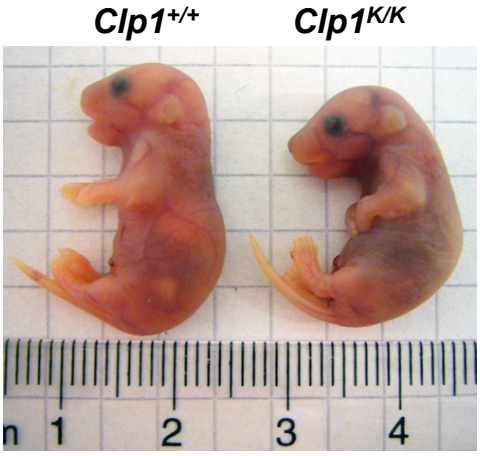

b

Growth and responsivity of *Clp1*$^{K/K}$ newborn pups

Genotype		*Clp1*$^{+/+}$ (n = 13)	*Clp1*$^{K/+}$ (n = 24)	*Clp1*$^{K/K}$ (n = 14)
Body weight (g)		1.17 ± 0.10	1.18 ± 0.06	1.02 ± 0.15**
Crown-Rump Length (cm)		2.21 ± 0.07	2.19 ± 0.06	2.06 ± 0.16**
Pinching response				
Neck	Strong	13	24	0
	Weak	0	0	12
	None	0	0	2
Tail	Strong	11	22	0
	Weak	2	2	12
	None	0	0	2

Supplementary Figure 3. Newborn *Clp1*$^{K/K}$ embryos exhibit reduced birth weights and hyporesponsiveness to pinching stimuli.

a, Appearance of E18.5 embryonic littermates. Note the lordotic body posture and dropping forelimbs in *Clp1*$^{K/K}$ embryos. A wild type littermate is shown as control. **b,** Birth weights, crown-rump lengths, and responses to pinching stimuli of newborn *Clp1*$^{+/+}$ and *Clp1*$^{K/K}$ littermates. All animals were tested for pinching responsiveness immediately after birth. Data are shown as mean values ± S.D. *P < 0.05,**P < 0.01, ***P < 0.001 (t-test).

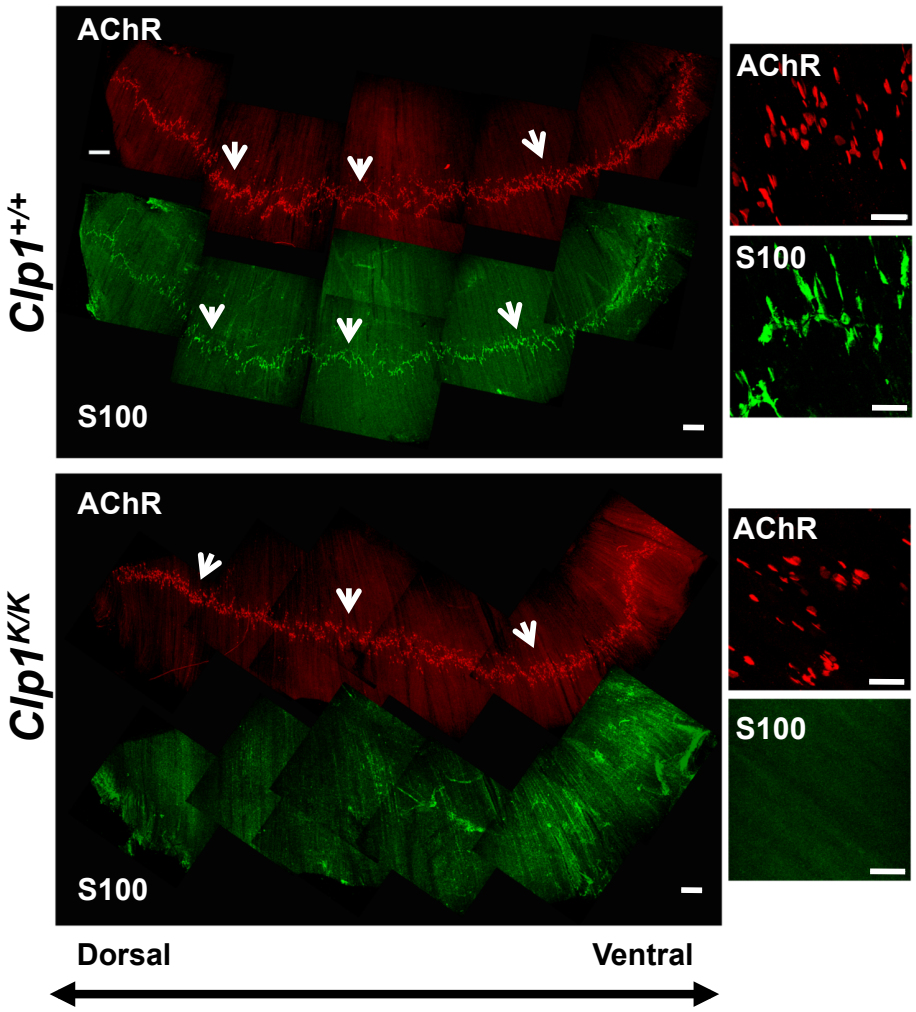

Supplementary Figure 4. Severe defects in neuromuscular junctions in the diaphragm of E18.5 *Clp1*$^{K/K}$ embryos.

Whole mount immunostaining of the diaphragm muscle of E18.5 *Clp1*$^{+/+}$ and *Clp1*$^{K/K}$ littermates showing postsynaptic acetylcholine receptor (AChR) clusters (red; α-Bungarotoxin) and Schwann cells marked with anti-S100 antibodies (green). Arrows indicate the characteristic central endplate zone. Note that S100 staining is absent in *Clp1*$^{K/K}$ embryos. Scale bars: left panels, 250 μm; right panels, 50 μm.

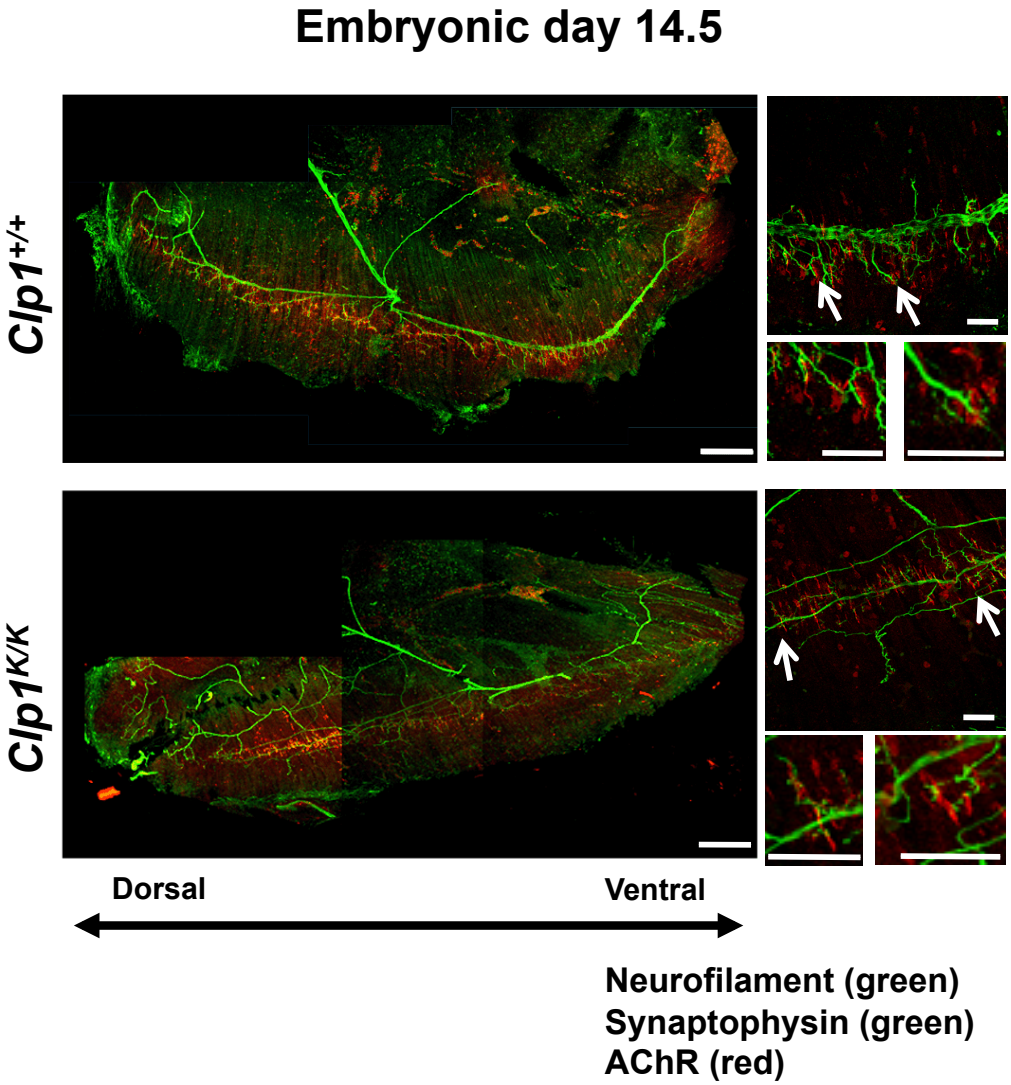

Supplementary Figure 5. Neuromuscular junctions in the diaphragm of E14.5 *Clp1*$^{K/K}$ embryos.

Whole mount immunostaining of the diaphragm muscle of E14.5 *Clp1*$^{+/+}$ and *Clp1*$^{K/K}$ littermates showing postsynaptic acetylcholine receptor (AChR) clusters (red; α-Bungarotoxin) and labeling of the phrenic nerve (green; dual anti-neurofilament and anti-synaptophysin staining). Note the defasciculation and mislocalization of the innervating nerve in *Clp1*$^{K/K}$ embryos, but apparently normal formation of neuromuscular junctions (arrows). Representative low and high magnification images are shown. Scale bars: left panels, 250 μm; right panels, 50 μm.

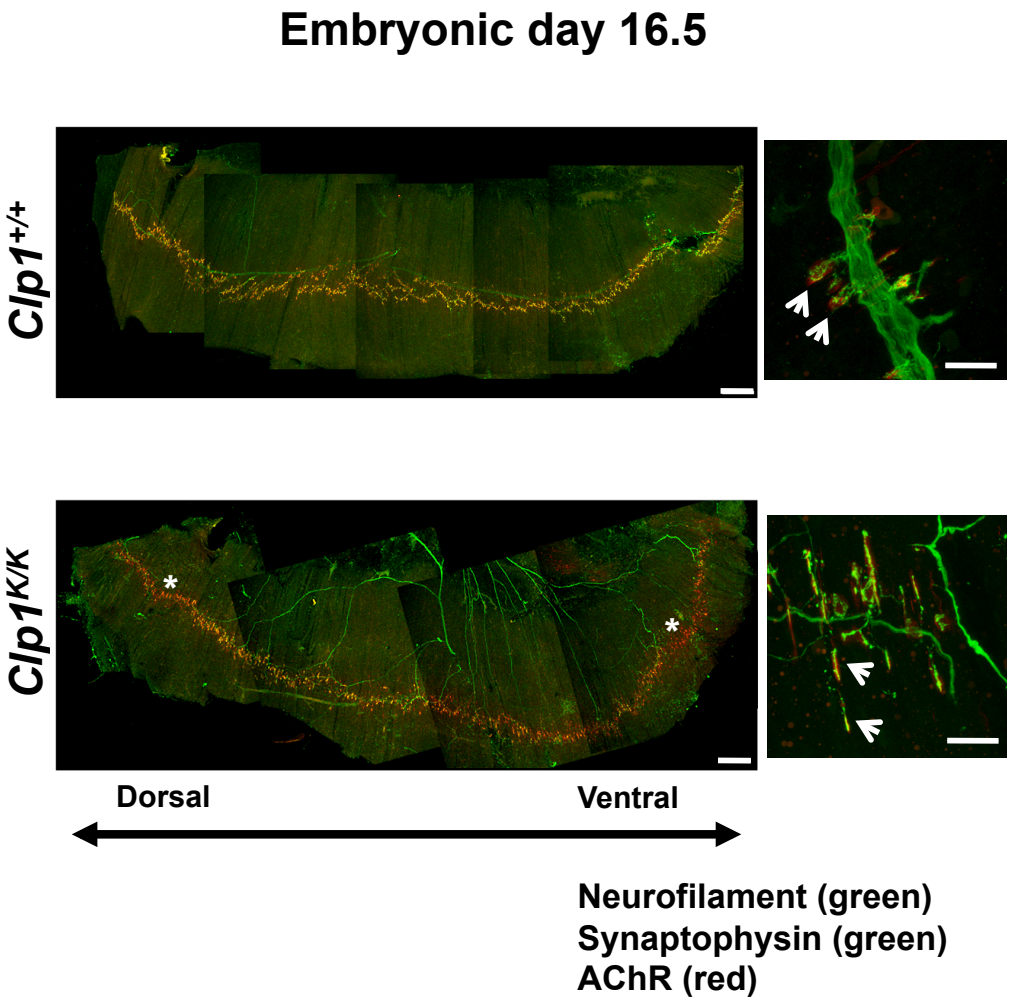

Supplementary Figure 6. Neuromuscular junctions in the diaphragm of E16.5 *Clp1*$^{K/K}$ embryos.

Whole mount immunostaining of the diaphragm muscle of E16.5 *Clp1*$^{+/+}$ and *Clp1*$^{K/K}$ littermates showing postsynaptic acetylcholine receptor (AChR) clusters (red; α-Bungarotoxin) and labeling of the phrenic nerve (green; dual staining for anti-neurofilament and anti-synaptophysin). Note that parts of the diaphragm have already become denervated in E16.5 *Clp1*$^{K/K}$ embryos (asterisks). Moreover, pronounced alterations in NMJ morphology can be detected (arrows). Representative low and high magnification images are shown. Scale bars: left panels, 250 μm; right panels, 25 μm.

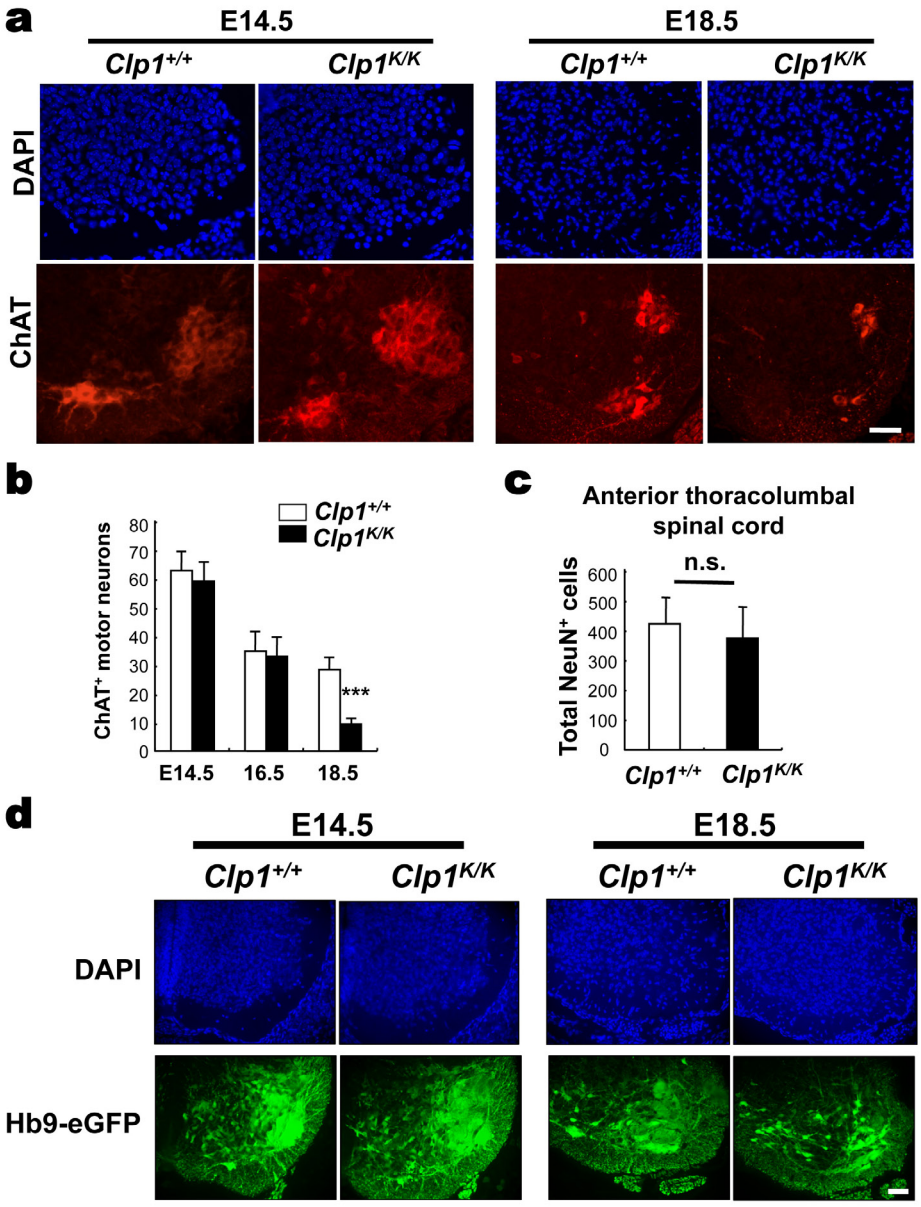

Supplementary Figure 7. Quantification of neurons in E18.5 *Clp1*$^{+/+}$ and *Clp1*$^{K/K}$ embryos.

a, Immunostaining for ChAT^{+} (red) motor neurons in the lumbar (L5) spinal cord of E14.5 and E18.5 *Clp1*$^{+/+}$ and *Clp1*$^{K/K}$ littermates on a C57BL/6 background. DAPI staining is shown to visualize nuclei. Note the apparently normal numbers of ChAT^{+} motor neurons on E14.5 but markedly reduced numbers of motor neuron in the spinal cord of *Clp1*$^{K/K}$ embryos on E18.5. Scale bar: 50 μm. **b,** Quantification of ChAT^{+} motor neurons in the lumbar (L5) spinal cord of E14.5, E16.5 and E18.5 *Clp1*$^{+/+}$ and *Clp1*$^{K/K}$ littermates. Data are from 5 mice per group and presented as mean values ± S.D. ***$P < 0.001$ (t-test). **c,** Quantification of total neuron numbers in the anterior thoracolumbar spinal cord of E18.5 *Clp1*$^{+/+}$ and *Clp1*$^{K/K}$ embryos using neuronal nuclear antigen (NeuN) as a marker. Data are from 3 embryos per group and presented as mean values ± S.D. No significant differences were detected among the groups (n.s.). **d,** Hb9-eGFP expressing neurons in the lumbar (L5) spinal cord of E14.5 and E18.5 *Clp1*$^{+/+}$ Hb9-eGFP and *Clp1*$^{K/K}$ Hb9-eGFP embryos on a C57BL/6 background. DAPI staining is shown to visualize nuclei. Note the markedly reduced numbers of ChAT^{+} motor neurons in the spinal cord of *Clp1*$^{K/K}$ Hb9-eGFP embryos on E18.5 as compared to E14.5. Scale bar: 50 μm.

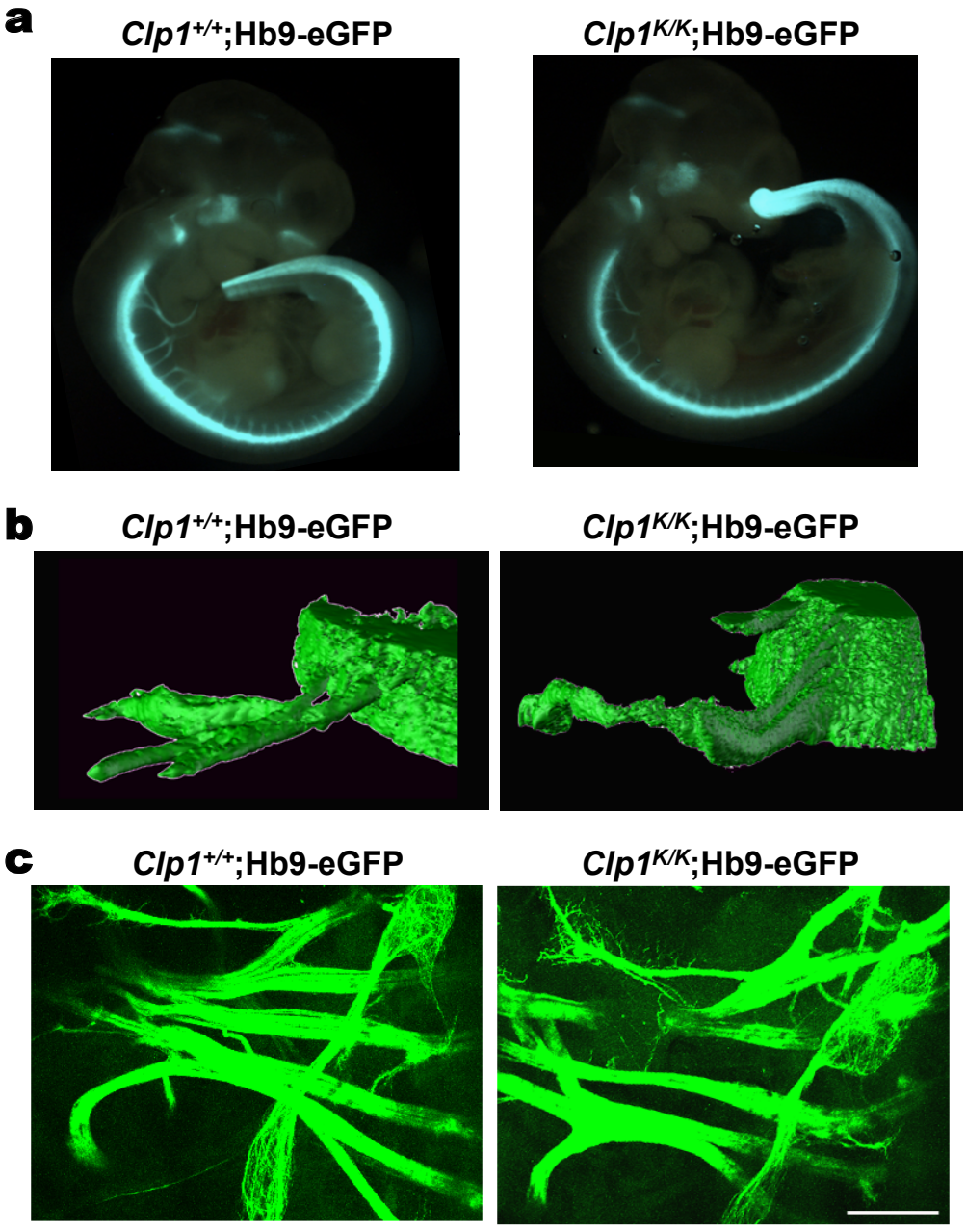

Supplementary Figure 8. Motor neuron pathfinding and motor axon development.

a, Neuron pathfinding and motor axon development in whole E10.5 *Clp1*$^{+/+}$ Hb9-eGFP and *Clp1*$^{K/K}$ Hb9-eGFP embryos on a C57BL/6 background. Note the apparently normal and segmented motor neuron outgrowth in *Clp1*$^{K/K}$ Hb9-eGFP mice. **b,** 3D reconstructions of axonal outgrowth at the thoracic region (T6-T7) of E12.5 *Clp1*$^{+/+}$ Hb9-eGFP and *Clp1*$^{K/K}$ Hb9-eGFP embryos. **c,** Pathfinding of motor neurons at the intercostal muscles in the cervical / high thoracic region of E12.5 *Clp1*$^{+/+}$ Hb9-eGFP and *Clp1*$^{K/K}$ Hb9-eGFP embryos. No apparent differences were detected between *Clp1*$^{+/+}$ and *Clp1*$^{K/K}$ littermates, indicating normal motor neuron pathfinding and apparently normal motor neuron development. Scale bar: 250 μm.

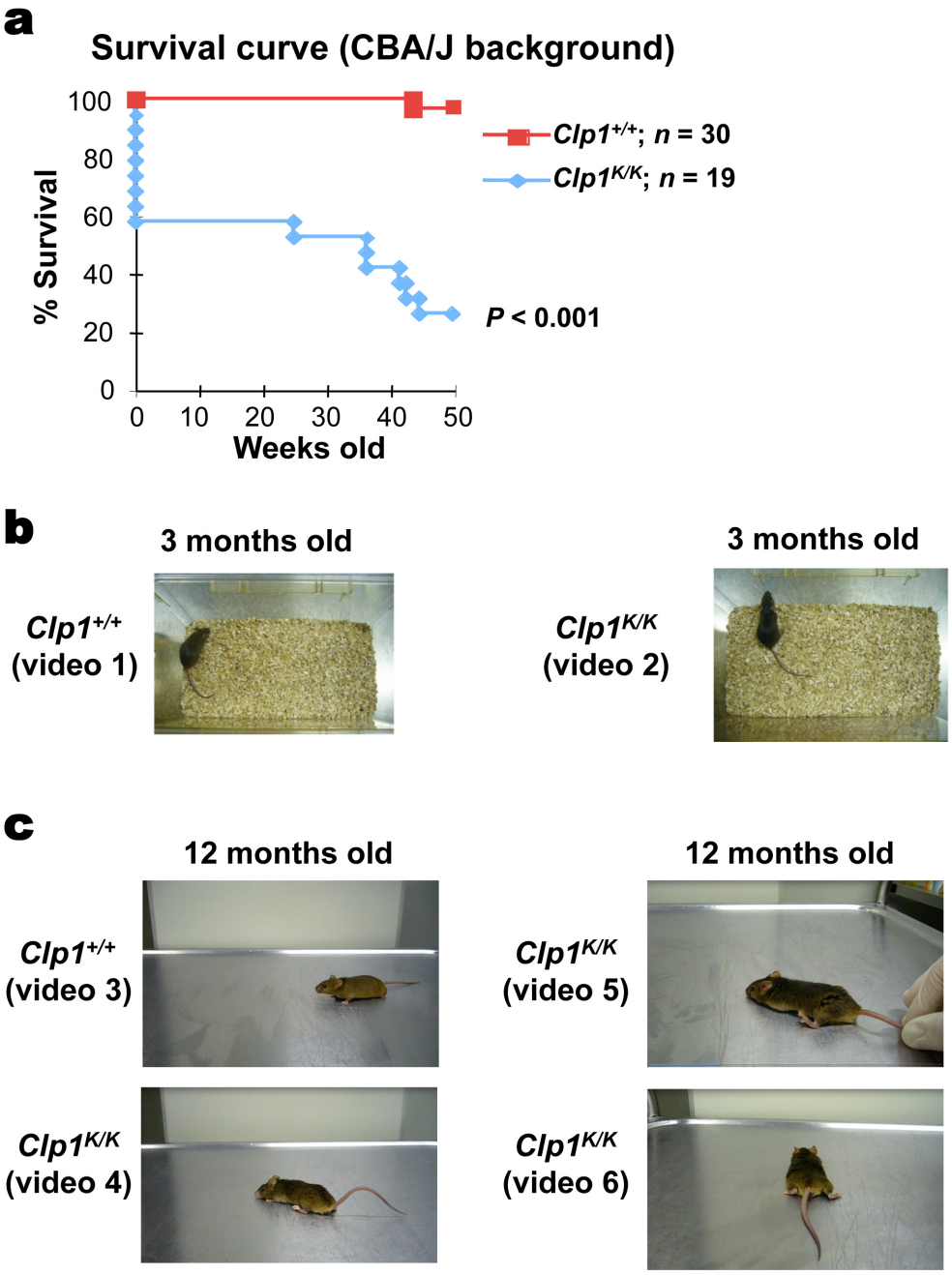

Supplementary Figure 9. Limb paralysis in viable *Clp1*$^{K/K}$ mice.

a, Survival curve of *Clp1*$^{+/+}$ and *Clp1*$^{K/K}$ mice on a CBA/J background. Mice were backcrossed for 5 generations. Survival curves were analyzed by log-rank tests using Kaplan-Meier survival curves. $P <$ 0.001 (log-rank test). **b,** Video 1 shows normal gait in a 3 months old control *Clp1*$^{+/+}$ mouse and video 2 shows ataxic gait in a 3 months old *Clp1*$^{K/K}$ littermate mouse. **c,** Video 3 shows normal gait in a 12 months old control *Clp1*$^{+/+}$ mouse. Videos 4-6 show severely impaired motor functions and limb paralysis in three different 12 months old *Clp1*$^{K/K}$ mice. Videos can be accessed via the Supplementary Information page.

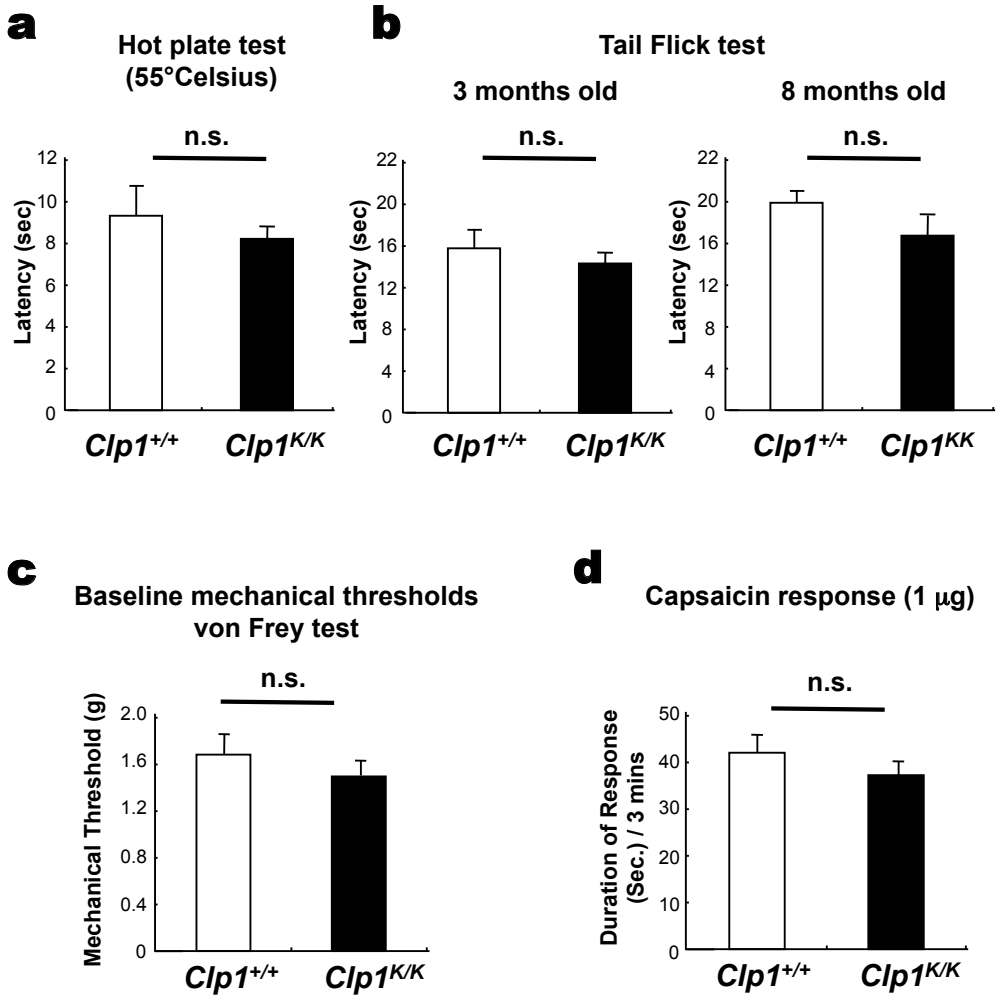

Supplementary Figure 10. Normal thermal, mechanical, and capsaicin sensory responses in *Clp1*$^{K/K}$ mice.

a,b, Thermal sensitivity. No differences were found in response latencies to the hot-plate test (55°C) (**a)** and tail flick test (**b).** Values represent the latency (seconds) to respond to the thermal stimulation. Data are from 8 mice per group at the indicated months of age and presented as mean values ± S.D. **c**, Mechanical thresholds determined in a von Frey test. Data are from 8 mice per group at 3 months of age and presented as mean values ± S.D. **d**, Intraplantar injection of capsaicin produced similar sensory responses in both cohorts of mice. Data are from 8 mice per group at 3 months of age and presented as mean values ± S.D. n.s., not significant.

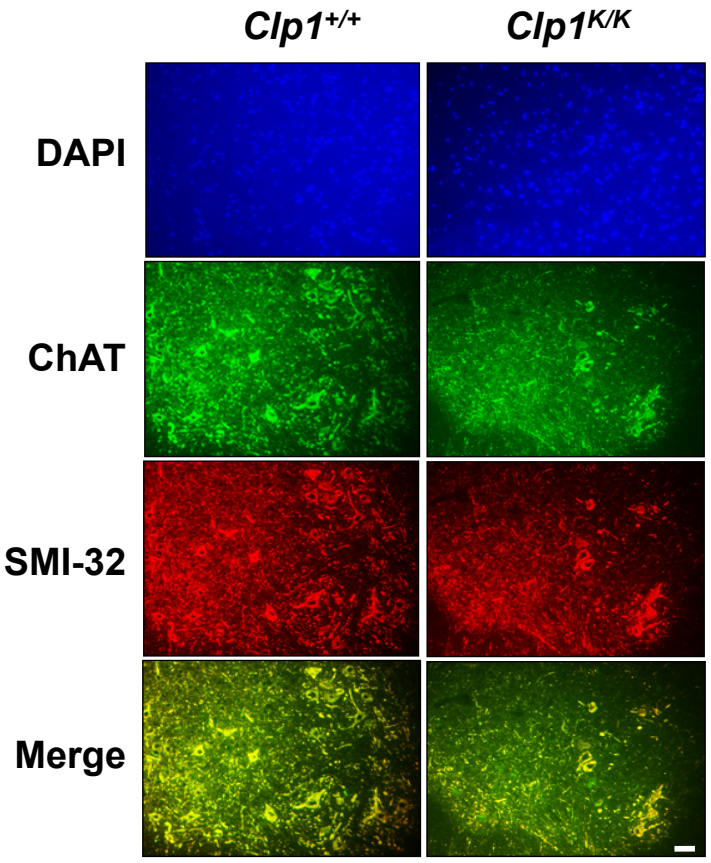

Supplementary Figure 11. Decreased motor neuron numbers in the spinal cord of viable *Clp1*$^{K/K}$ mice.

Immunostaining for motor neurons in the lumbar (L5) spinal cord of 4 months old *Clp1*$^{+/+}$ and *Clp1*$^{K/K}$ littermates on a CBA/J background using antibodies to the prototypic motor neuron markers ChAT (green) and SMI-32 (red). DAPI staining is shown to visualize nuclei. Scale bar: 50 μm.

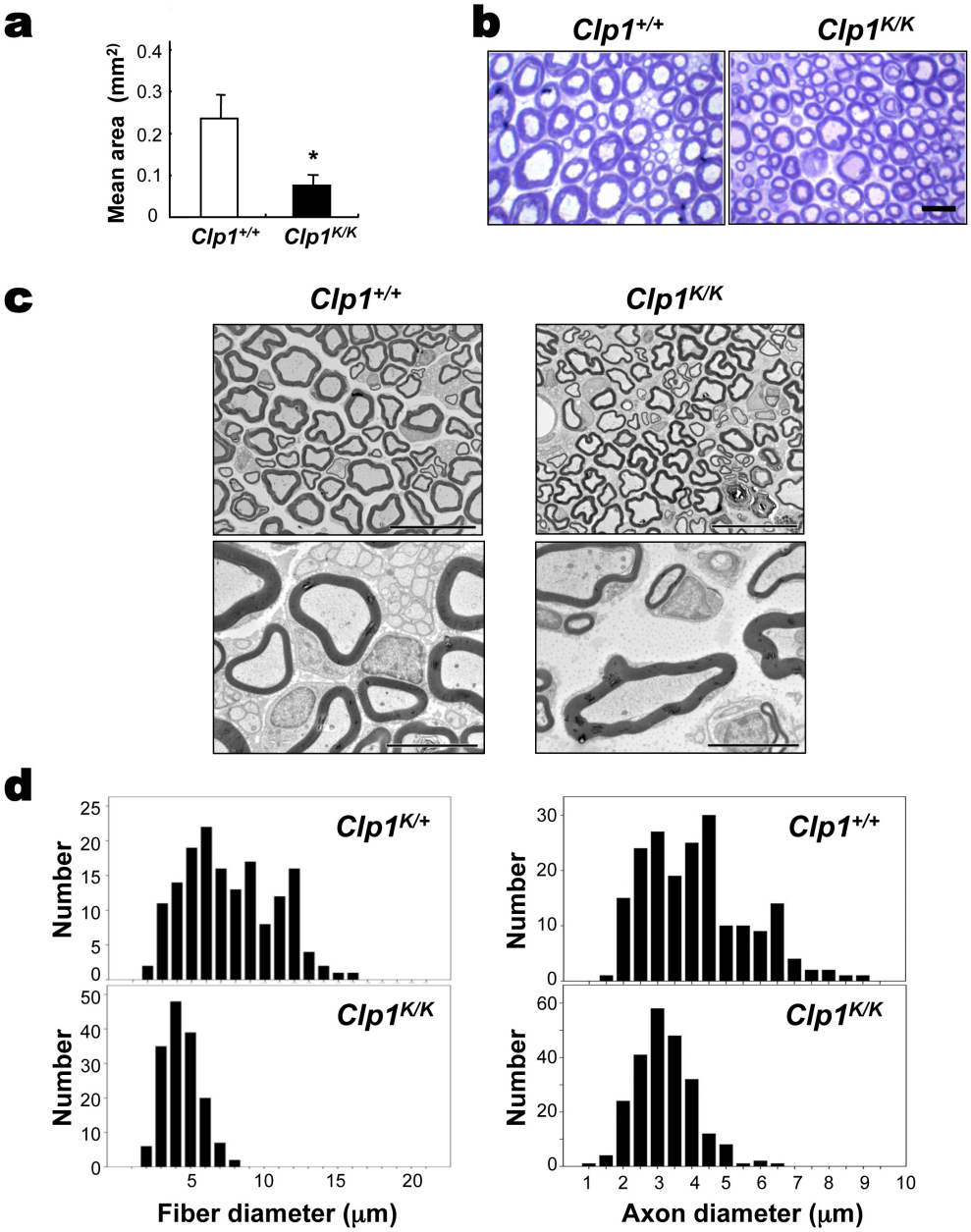

Supplementary Figure 12. Sciatic nerve degeneration and loss of large size motor fibers in *Clp1*$^{K/K}$ mice.

a, Quantification of the cross-sectional area in the distal parts of the sciatic nerve of 4 months old *Clp1*$^{+/+}$ and *Clp1*$^{K/K}$ littermates. Data are from 3 mice per group and presented as mean values ± S.D. *P < 0.05 (t-test). **b**, Toluidine blue staining of semi-thin distal sciatic nerve sections from 4 months old *Clp1*$^{+/+}$ and *Clp1*$^{K/K}$ littermates. Note the marked reduction in large fibers. Scale bar: 10 μm. **c**, Transmission electron micrographs of the sciatic nerve from 4 months old *Clp1*$^{+/+}$ and *Clp1*$^{K/K}$ littermates. Note apparently normal myelination and regular myelin sheaths in the surviving *Clp1*$^{K/K}$ sciatic nerve fibers. Scale bars: upper panels: 20 μm, lower panels: 5 μm. **d,** Histograms depicting the axonal and nerve fiber diameter frequencies in the sciatic nerves of 4 months old *Clp1*$^{K/+}$, *Clp1*$^{+/+}$ and *Clp1*$^{K/K}$ littermates. Data are from 3 mice per group. Note the decreased numbers of larger-diameter nerve fibers and axons in *Clp1*$^{K/K}$ mice compared to *Clp1*$^{K/+}$ and *Clp1*$^{+/+}$ littermate controls.

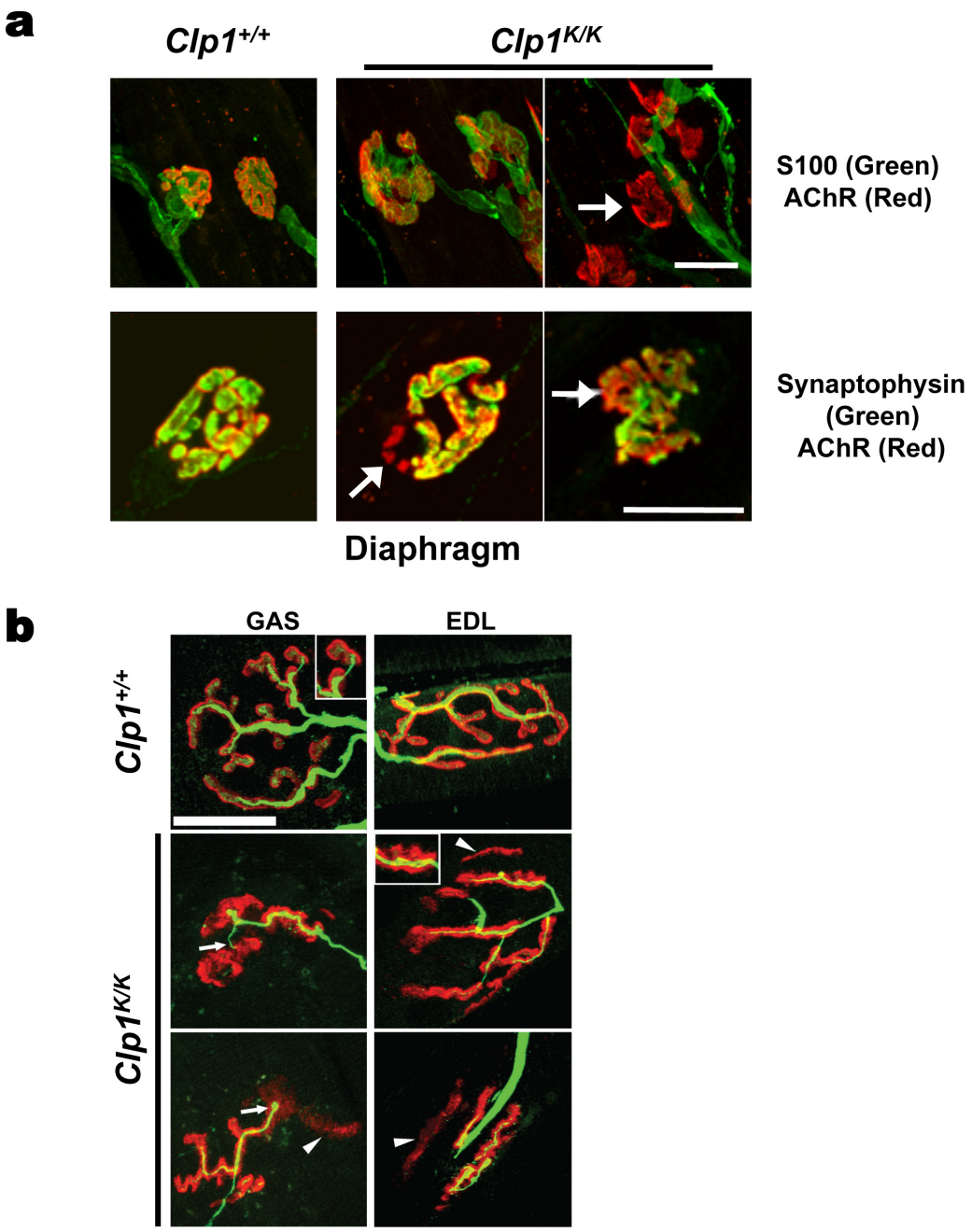

Supplementary Figure 13. Fragmentation of existing neuromuscular junctions in *Clp1*$^{K/K}$ mice.

a,b, Whole mount immunostaining for post-synaptic acetycholine receptors (AChRs) (red; α-Bungarotoxin) and S100–marked Schwann cells (green) or pre-synaptic terminals labeled by anti-synaptophysin / neurofilament (green) in the (**a**) diaphragm, **(b)** gastrocnemius muscle (GAS) and extensior digitorum longus (EDL) of 5 months (a) and 12 months (b) old *Clp1*$^{+/+}$ and *Clp1*$^{K/K}$ littermates. Note that in *Clp1*$^{K/K}$ mice neuromuscular junctions are partially denervated (arrows) resulting in fragmentation and disassembly (arrowheads). Magnified insets show the characteristic smooth outline of AChR borders in wild-type muscle compared to the frayed appearance of AChR borders in *Clp1* mutant muscle. Scale bars: 25 μm.

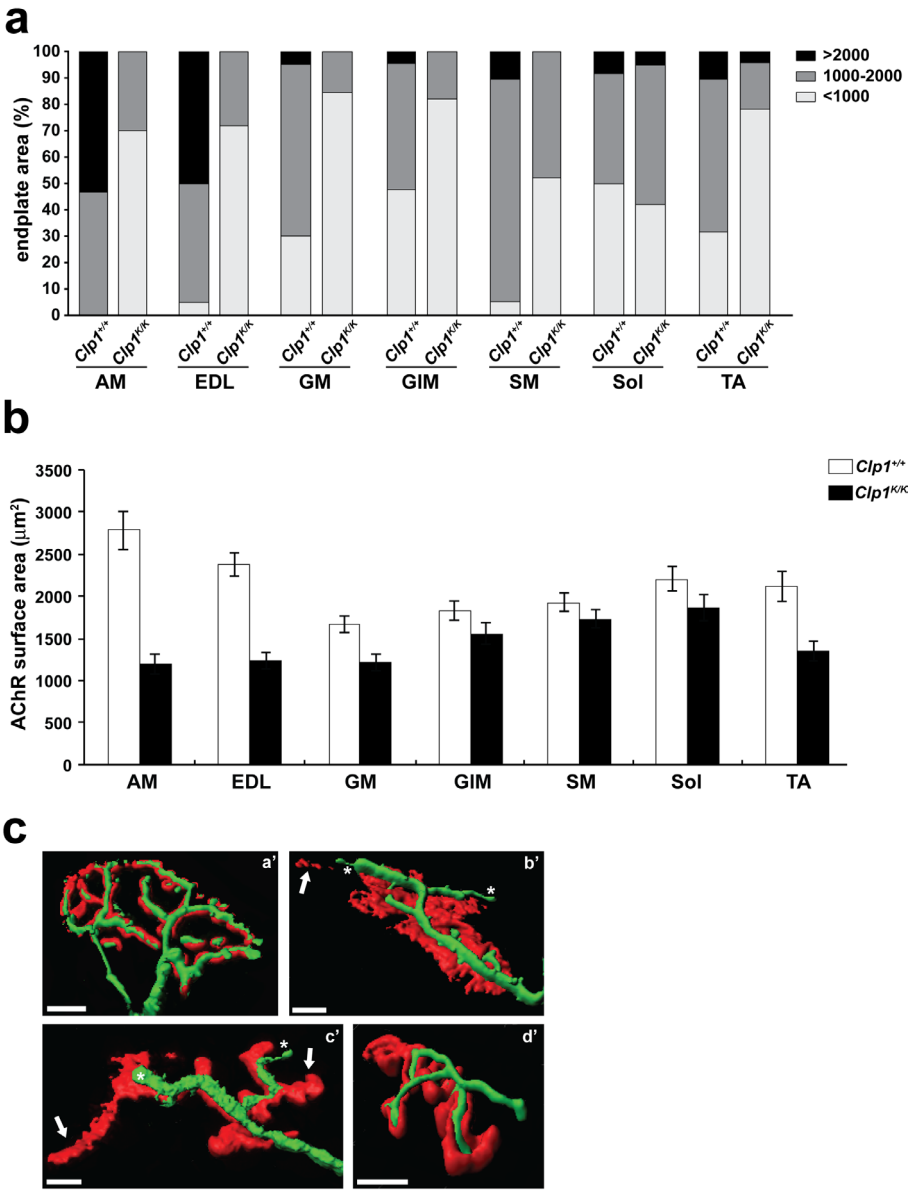

Supplementary Figure 14. Assessment of neuromuscular junctions in different muscle groups from *Clp1*$^{K/K}$ mice.

a, Quantification of endplate areas from *en face* NMJs revealing a loss of large size NMJs from the indicated *Clp1*$^{K/K}$ muscles. Note the normal NMJ size in the *Clp1*$^{K/K}$ soleus muscle. Endplates were categorized into three classes: small (<1000 µm^2), normal-sized (1000-2000 µm^2) and large (>2000 µm^2). n = 10 (from 12 months old mice). **b,** The AChR surface area calculated from 3D reconstructions was reduced in the indicated muscles from *Clp1*$^{K/K}$ mice demonstrating a fragmentation and/or loss of AChRs. n = 10 (from 12 months old mice). **c**, Representative 3D reconstructions from wild-type (a') and mutant (b'-d') muscles stained with anti-synapsin/neurofilament (green) and α-Bungarotoxin (red). Denervation and AChR dispersal are marked with asterisks and arrows, respectively. Scale bars: 10 µm. Data from 12 months old mice are shown. AM; adductus muscle, EDL, extensor digitorum longus muscle, GM; gastrocnemius muscle, GlM; gluteus muscle, SM; sternomastoid muscle, Sol; soleus muscle; TA, tibialis anterior muscle.

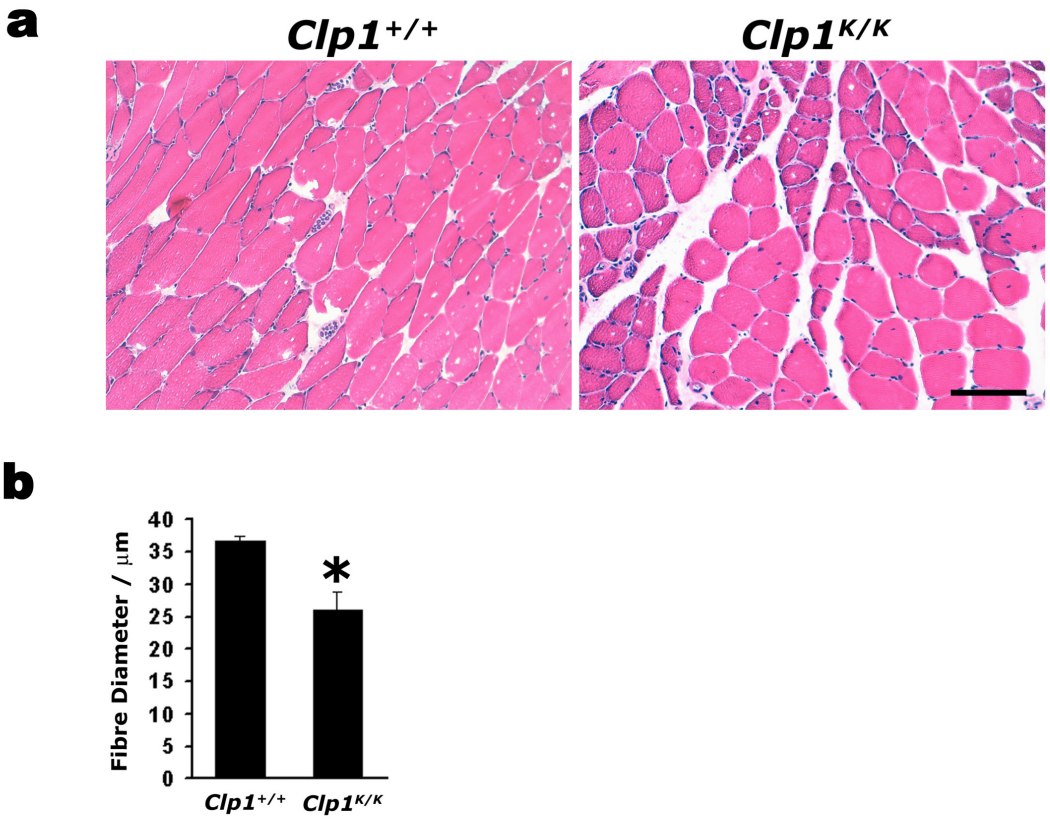

Supplementary Figure 15. Neurogenic muscle atrophy in *Clp1*$^{K/K}$ mice.

a, H&E staining of the gastrocnemic muscle of adult *Clp1*$^{K/K}$ and control *Clp1*$^{+/+}$ mice is shown. Note the grouped atrophic fibres in *Clp1*$^{K/K}$ mice, indicative of neurogenic atrophy. Scale bar: 100 µm. **b,** The bar graph shows decreased mean fiber size in *Clp1*$^{K/K}$ versus control *Clp1*$^{+/+}$ mice. Mean fibre diameters ± S.E.M. are shown for 3 mice in each experimental group. * $P < 0.05$.

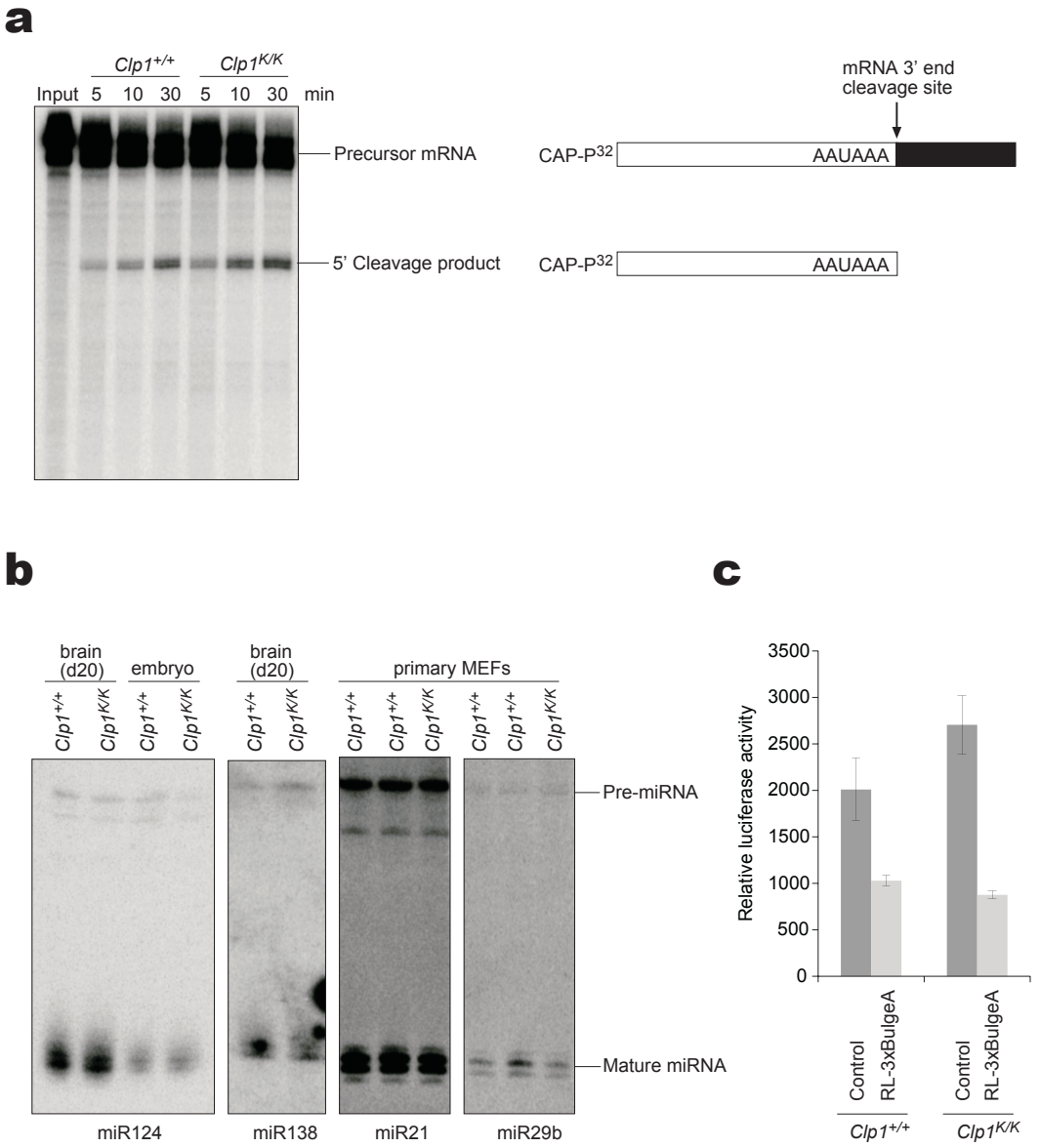

Supplementary Figure 16. The CLP1 K127A mutation does not impair mRNA 3' end cleavage *in vitro* nor affects miRNA processing.

a, Nuclear extracts were generated from *Clp1*$^{+/+}$ and *Clp1*$^{K/K}$ MEFs and incubated with 5' CAP-labeled SV40 late precursor mRNA. mRNA cleavage at the poly(A) site was monitored at the indicated time points. **b**, Northern blot analysis of levels of the indicated miRNAs using total brain (20 days old mice), total embryonic tissue (embryo, E18.5), and primary MEFs derived from *Clp1*$^{+/+}$ and *Clp1*$^{K/K}$ mice. Mature miRNAs and pre-miRNAs are indicated. **c**, Dual-luciferase reporter assay to assess let-7a miRNA function. *Clp1*$^{+/+}$ and *Clp1*$^{K/K}$ MEFs were transfected with an expression vector for *Renilla* luciferase (RL) with or without (control) three bulged binding sites for let-7a miRNA at the 3'-UTR. The activity of the RL reporter is plotted relative to firefly luciferase activity encoded by the co-transfected vector pGL3. All transfections were performed in triplicate of which the data are represented as mean values.

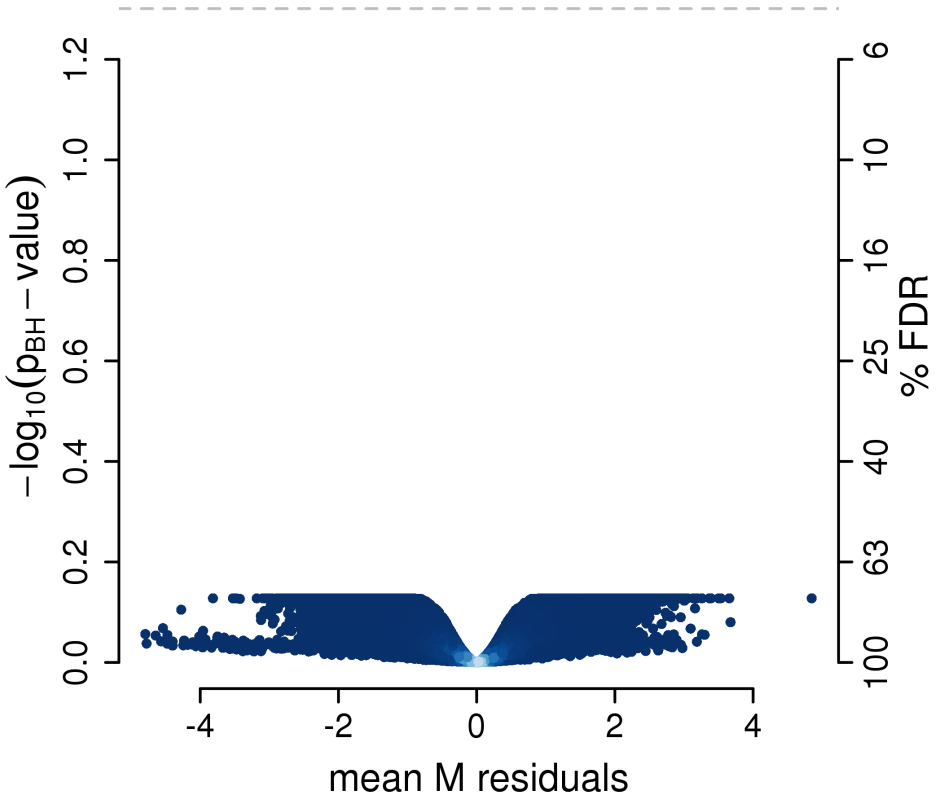

Supplementary Figure 17. Normal differential splicing in *Clp1*$^{K/K}$ mice.

The Volcano plot summarizes the results from the differential splicing analyses using Affymetrix Exon microarrays. The difference of expression of a part or a full exon relative to the expression of its gene between spinal cord tissue from *Clp1*$^{K/K}$ and wild-type mice (CBA/J background, 16 days after birth) is shown on the x-axis and the significance of this difference on the y-axis. Significantly differential spliced exons would show up in the left and right upper corners of the plot. For a detailed description of the analysis see the supplementary Methods[25]. M residuals: average $\log_2$ difference of probe residuals; p_{BH}: p-values adjusted for multiple hypothesis testing with the method of Benjamini and Hochberg; FDR: false discovery rate. The dashed grey line represents a 5% FDR (p_{BH}=0.05). All primary exon array data have been deposited to Gene Expression Omnibus (http://www.ncbi.nlm.nih.gov/geo/query/acc.cgi?token=znqpxiukwocyefi&acc=GSE35924).

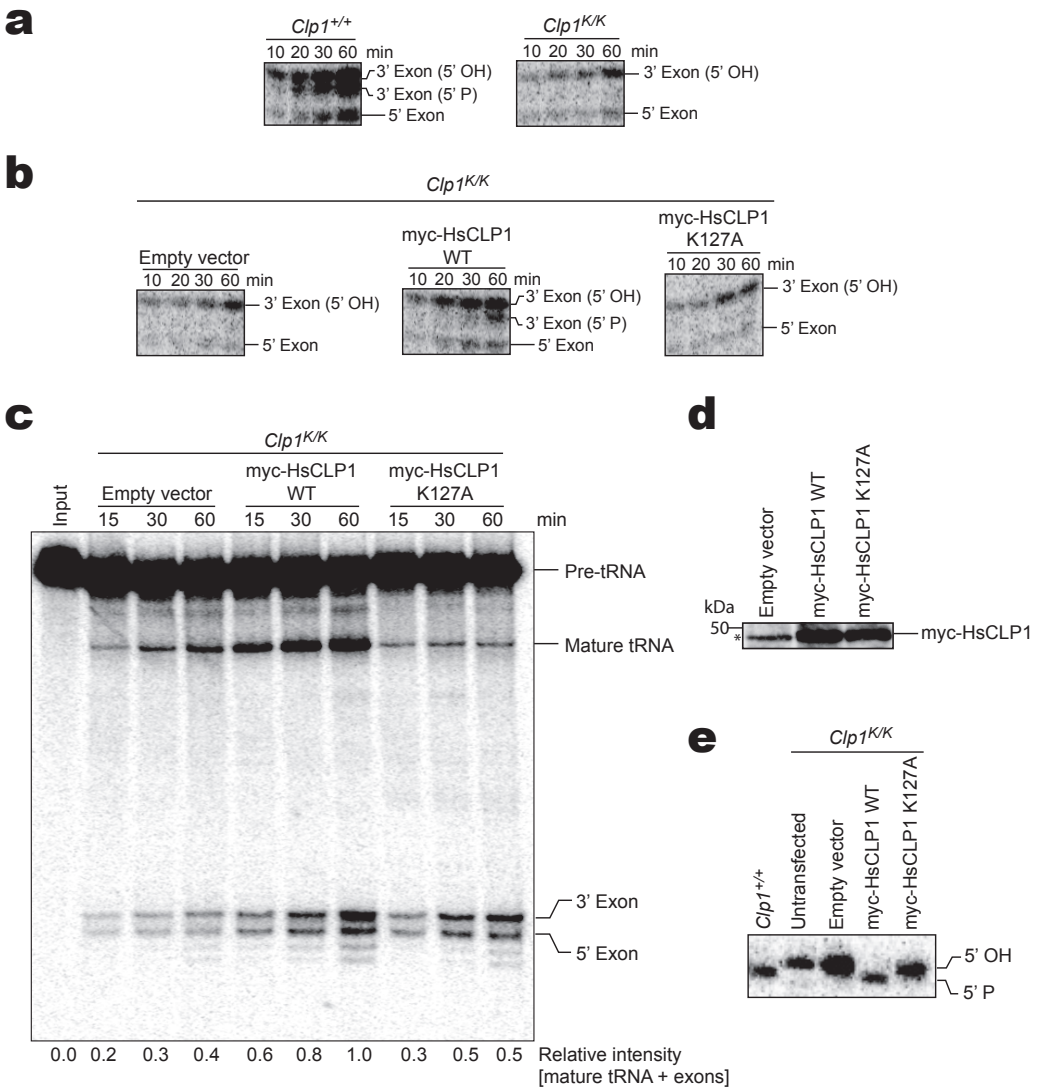

Supplementary Figure 18. Ectopic expression of wild type but not the CLP1 K127A mutant rescues impaired exon generation in *Clp1*$^{K/K}$ MEFs.

a,**b**, An internally labeled intron-containing pre-tRNA^{Phe} was incubated with nuclear extracts from **a,** immortalized *Clp1*$^{+/+}$ and *Clp1*$^{K/K}$ MEFs and **b,** from *Clp1*$^{K/K}$ MEFs transiently transfected with an empty vector or plasmids encoding myc-tagged human (Hs) wild type (WT) CLP1, or myc-tagged K127A CLP1. Pre-tRNA processing and 5' phosphorylation of the 3' exon were monitored by electrophoresis. **c**, An internally labeled intron-containing pre-tRNA^{Phe} was incubated with nuclear extracts from *Clp1*$^{K/K}$ MEFs transiently transfected with an empty plasmid, or plasmids encoding WT and K127A HsCLP1. Pre-tRNA processing was monitored by electrophoresis. Relative intensity values (N) were calculated as follows: N=[intensities (mature tRNA + 3' exon + 5'exon) at a certain time point] / [intensities (mature tRNA + 3' exon + 5' exon) at 60 min for WT HsCLP1]; the latter was arbitrarily set to 1.0. **d**, Similar levels of myc-tagged WT and K127A HsCLP1 in the nuclear extracts used for the experiment in **b** and **c** were confirmed by anti-myc Western blotting. The asterisk (*) denotes an unrelated band that co-migrates with HsCLP1. **e**, CLP1 RNA-kinase activity was assayed by incubating a 3' end labeled, 5' OH group containing RNA duplex for 60 min with the extracts used in **b**. Extracts from *Clp1*$^{+/+}$ MEFs were used as control. Phosphorylation was monitored by electrophoresis.

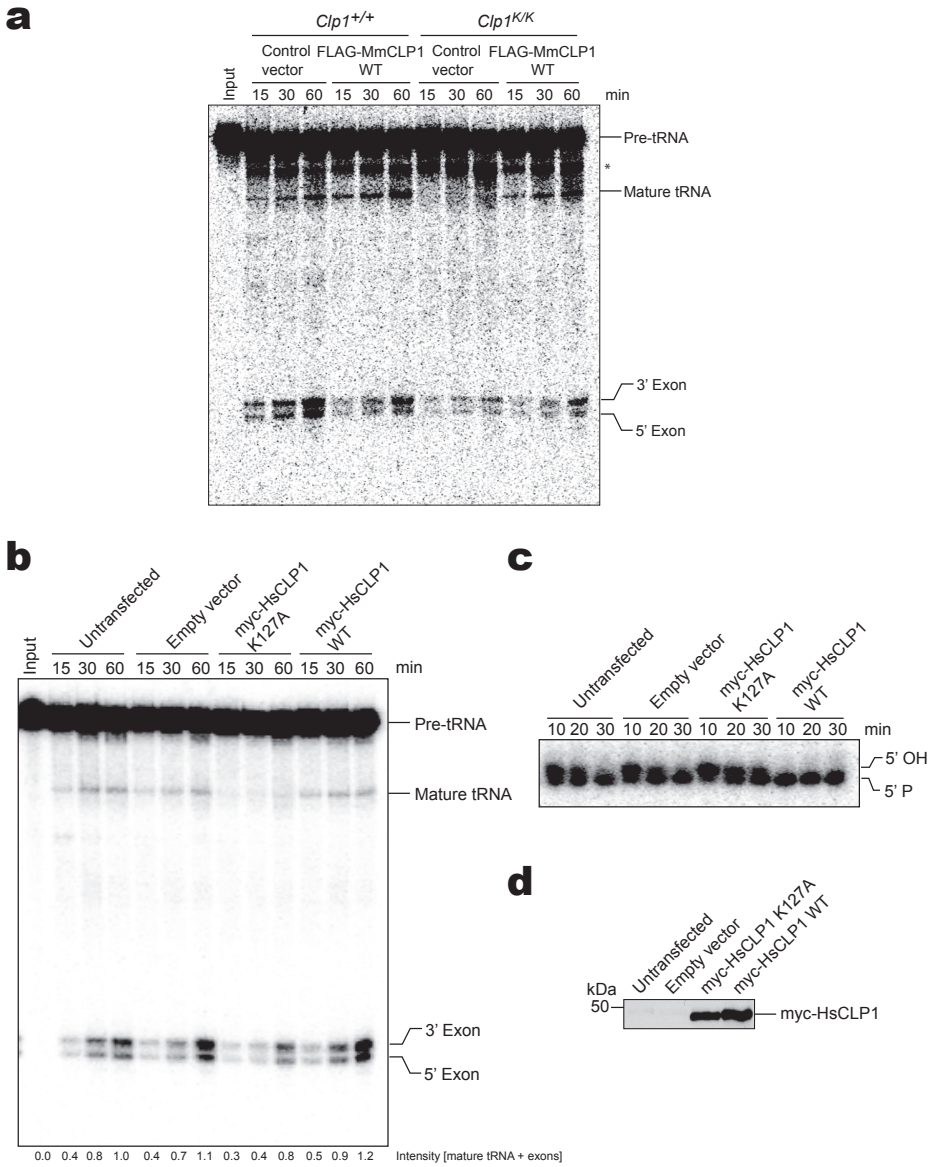

Supplementary Figure 19. Restoration of pre-tRNA processing in *Clp1*$^{K/K}$ MEFs stably expressing wild type CLP1.

a, An internally labeled intron-containing pre-tRNA^{Phe} was incubated with nuclear extracts derived from immortalized *Clp1*$^{+/+}$ and *Clp1*$^{K/K}$ MEFs retrovirally infected with a control vector or an expression vector encoding Flag-tagged mouse (Mm) wild type (WT) CLP1. Pre-tRNA processing was monitored by electrophoresis. The asterisk (*) denotes an unrelated band. **b**, An internally labeled intron-containing pre-tRNA^{Phe} was incubated with whole cell extracts from untransfected HeLa cells and HeLa cells transiently transfected with an empty plasmid, or plasmids encoding myc-tagged human (Hs) WT and K127A CLP1. Pre-tRNA processing was monitored by electrophoresis. Intensity values (N) were calculated as follows: N=[intensities (mature tRNA + 3' exon + 5'exon) at certain time point] / [intensities (mature tRNA + 3' exon + 5' exon) at 60 min for untransfected HeLa cells]; the latter was arbitrarily set to 1.0. **c**, RNA-kinase activity was assayed by incubating a 3' end labeled 5' OH group containing RNA duplex with the extracts used in **b** for the times indicated. Phosphorylation was monitored by electrophoresis at the indicated time points. Note that CLP1 K127A functions in a dominant negative manner. **d**, Similar levels of WT and K127A HsCLP1 in extracts used in **b** were confirmed by anti-myc Western blotting**.**

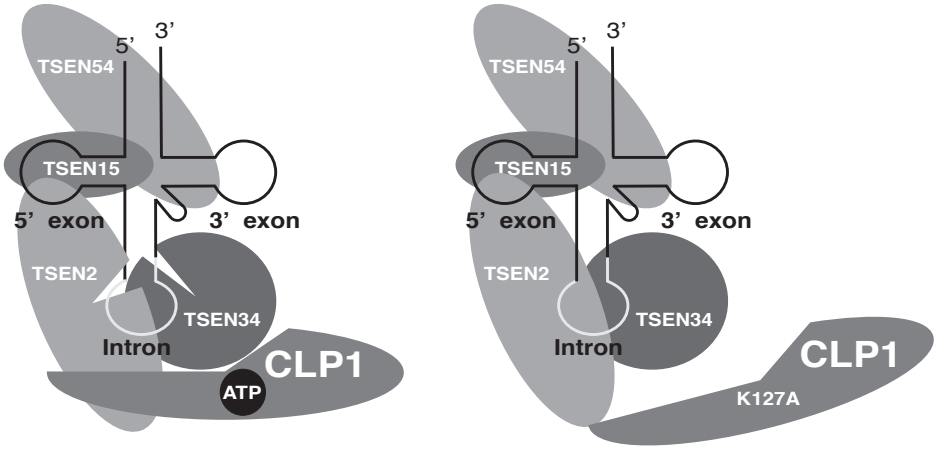

ATP binding/hydrolysis by CLP1

Binding of CLP1 to TSEN.
Efficient pre-tRNA cleavage.

No ATP binding/hydrolysis by CLP1

Reduced binding of CLP1 to TSEN.
Inefficient pre-tRNA cleavage.

Supplementary Figure 20. Model for the potential role of CLP1 in pre-tRNA cleavage.

A graphical representation of the tRNA splicing endonuclease (TSEN) in complex with CLP1. On the left, wild type CLP1 is able to bind/hydrolyze ATP and the TSEN complex is efficient in processing pre-tRNAs. On the right, a mutation in the active site of CLP1 that abolishes ATP binding/hydrolysis leads to the formation of a defective TSEN complex that is impaired in pre-tRNAs processing.

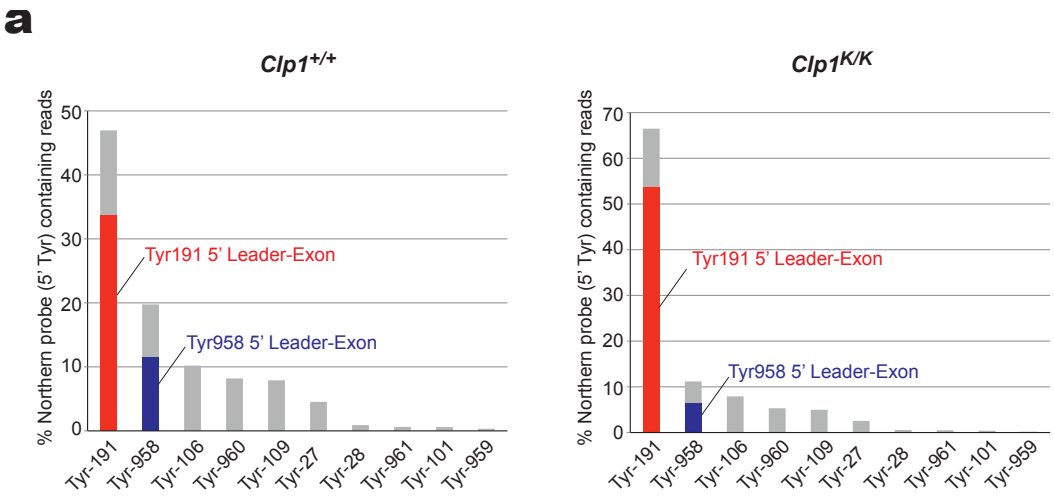

	5'Leader 5'Exon	Clp1+/+	Clp1K/K
Tyr191-5' Leader-Exon fragment	GUGCUUCCCUUCGAUAGCUCAGCU**GGUAGAGCGGAGGACUGUAG**	33.7% (27216)	53.6% (54753)
Tyr958-5' Leader-Exon fragment	GUGGAUCCUUCGAUAGCUCAGUU**GGUAGAGCGGAGGACUGUAG**	11.5% (9313)	6.4% (6529)
Northern probe sequence (reverse complementary)	5'-**GGTAGAGCGGAGGACTGTAG**-3'		

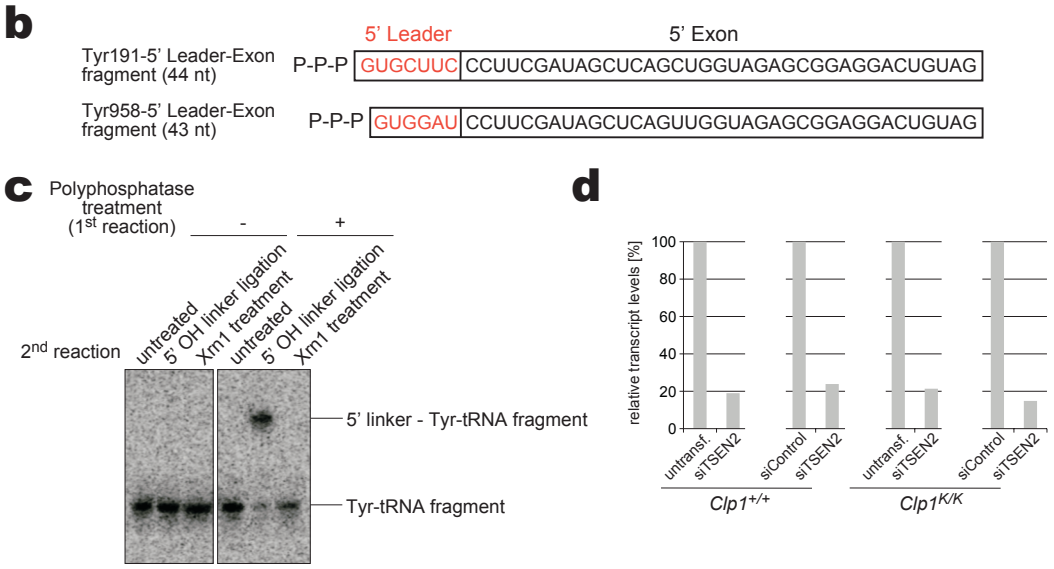

Supplementary Figure 21. Tyrosine tRNA fragments are mainly derived from tRNA191-TyrGTA and tRNA958-TyrGTA.

a, The bulk of the RNA at ~41-46-nts detected with the tyrosine (Tyr) tRNA 5' exon DNA/LNA Northern probe corresponds to the 5' leader-exon sequence of tRNA191-TyrGTA and tRNA958-TyrGTA. Total RNA from *Clp1*$^{+/+}$ and *Clp1*$^{K/K}$ MEFs was isolated and separated in a 10% denaturing polyacrylamide gel. The gel slices containing RNA of 37-50 nt were isolated, RNA was purified and

treated with tobacco acid pyrophosphatase to hydrolyze the terminal 5' triphosphate group of tRNAs. 5' and 3'adapter oligonucleotides were ligated, cDNA was prepared, PCR amplified and subjected to Illumina sequencing. Reads were genomically aligned by overlap with tRNA locations (Lowe lab, http://gtrnadb.ucsc.edu/Mmusc/Mmusc-by-locus-txt.html). The relative contribution of number of reads that contain the Tyr-tRNA-5'exon Northern probe sequence was plotted for each Tyr-tRNA subclass (graph). The two most abundant tRNA species amongst the reads in both $Clp1^{+/+}$ and $Clp1^{K/K}$ MEFs were derived from *M. musculus* chr14.trna191-TyrGTA (Tyr191 5' Leader-Exon fragment) and *M. musculus* chr13.trna958-TyrGTA (Tyr958 5' Leader-Exon fragment; mouse July 2007 (mm9) genome assembly). Table: numbers in percentage are related to the total number of Tyr-tRNA-5' exon Northern probe sequence-containing reads, numbers in brackets represent the absolute read numbers. **b**, Sequences and 5' end modification of the Tyr191 and Tyr958 5' leader-exon fragments. **c**, The Tyr-tRNA fragment contains a 5' triphosphate group. Size-selected purified total RNA from $Clp1^{K/K}$ MEFs containing Tyr-tRNA fragments was left untreated or treated with polyphosphatase and then either treated with the 5' phosphate-specific recombinant exonuclease Xrn1 or incubated with a 5' OH-terminated RNA linker in the presence of T4 RNA ligase. Northern blot analysis of the reaction products was performed using a DNA/LNA probe complementary to the 5' exon of Tyr-tRNA. **d**, Confirmation of the RNAi-mediated depletion of TSEN2 in $Clp1^{+/+}$ and $Clp1^{K/K}$ MEFs by quantitative polymerase chain reaction (qPCR) of the experiment described in Fig. 4f. TSEN2 transcript levels were plotted relative to levels in untransfected or control siRNA transfected cells. Results are depicted as mean values of triplicate PCR reactions.

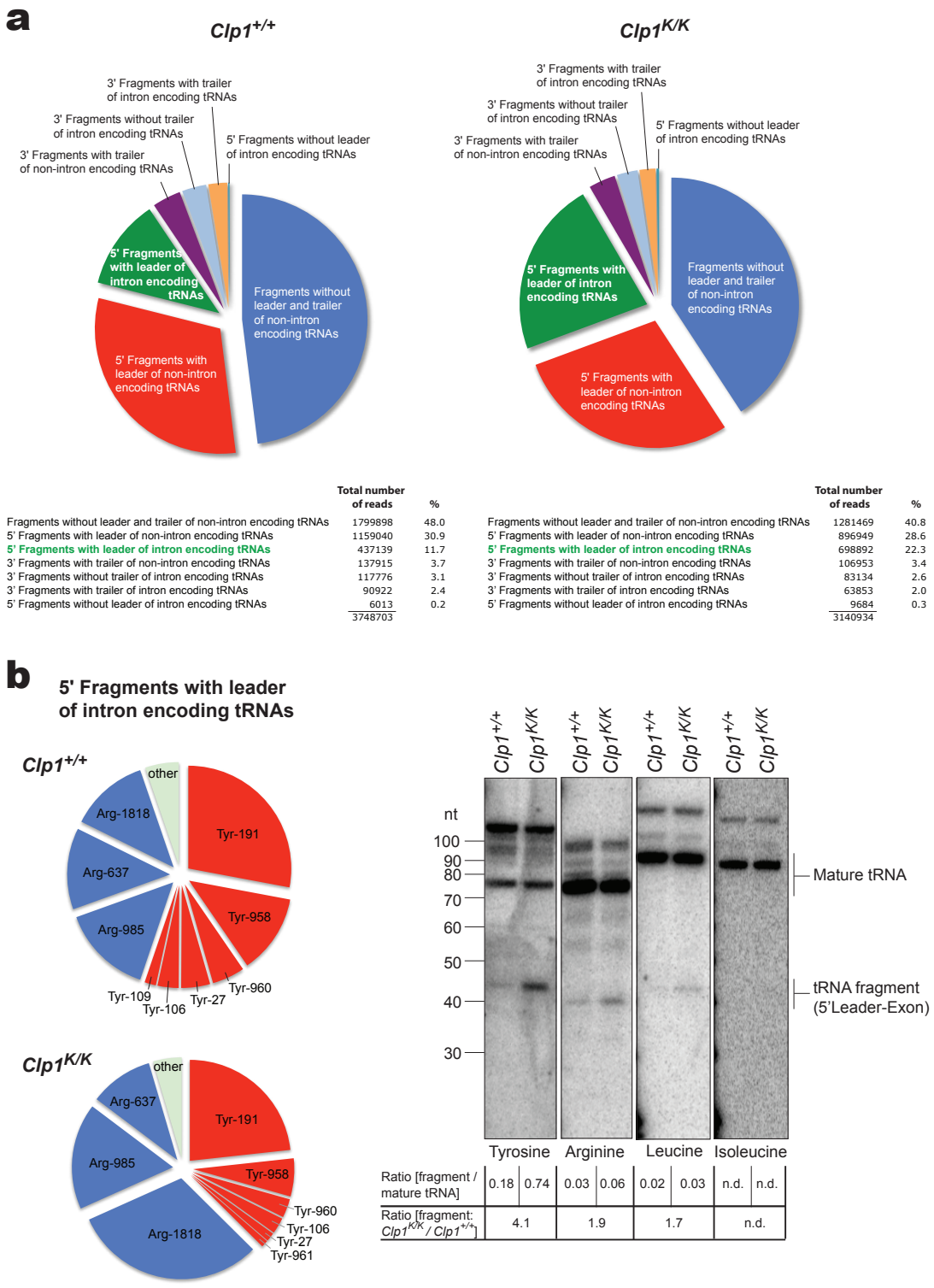

	Total number of reads	%
Fragments without leader and trailer of non-intron encoding tRNAs	1799898	48.0
5' Fragments with leader of non-intron encoding tRNAs	1159040	30.9
5' Fragments with leader of intron encoding tRNAs	437139	11.7
3' Fragments with trailer of non-intron encoding tRNAs	137915	3.7
3' Fragments without trailer of intron encoding tRNAs	117776	3.1
3' Fragments with trailer of intron encoding tRNAs	90922	2.4
5' Fragments without leader of intron encoding tRNAs	6013	0.2
	3748703	

	Total number of reads	%
Fragments without leader and trailer of non-intron encoding tRNAs	1281469	40.8
5' Fragments with leader of non-intron encoding tRNAs	896949	28.6
5' Fragments with leader of intron encoding tRNAs	698892	22.3
3' Fragments with trailer of non-intron encoding tRNAs	106953	3.4
3' Fragments without trailer of intron encoding tRNAs	83134	2.6
3' Fragments with trailer of intron encoding tRNAs	63853	2.0
5' Fragments without leader of intron encoding tRNAs	9684	0.3
	3140934	

	Tyrosine		Arginine		Leucine		Isoleucine	
Ratio [fragment / mature tRNA]	0.18	0.74	0.03	0.06	0.02	0.03	n.d.	n.d.
Ratio [fragment: $Clp1^{K/K}$ / $Clp1^{+/+}$]	4.1		1.9		1.7		n.d.	

Supplementary Figure 22. Accumulation of tyrosine tRNA fragments.

a, Uniquely genomically aligned reads of the RNA library derived from *Clp1*$^{+/+}$ and *Clp1*$^{K/K}$ MEFs were bioinformatically analysed and assigned by overlap with tRNA locations (http://gtrnadb.ucsc.edu/Mmusc/Mmusc-by-locus-txt.html) to seven classes: A) 5' fragments with leader of intron encoding tRNAs; B) 5' fragments without leader of intron encoding tRNAs; C) 5'

fragments with leader of non-intron encoding tRNAs; D) 3' fragments with trailer of intron encoding tRNAs; E) 3' fragments without trailer of intron encoding tRNAs; F) 3' fragments with trailer of non-intron encoding tRNAs; G) fragments without leader and trailer of non-intron encoding tRNAs. Pie charts and tables show the contribution of aligned reads to each class. **b,** The predominant leader-containing tRNA 5' fragment species accumulating in $Clp1^{K/K}$ MEFs are derived from Tyr-tRNAs. The relative abundance of tRNA species, present in the RNA library derived from $Clp1^{+/+}$ and $Clp1^{K/K}$ MEFs and assigned to the class "5' fragments with leader of intron encoding tRNAs", is represented as pie charts (left panels). Northern analysis on RNA from $Clp1^{+/+}$ and $Clp1^{K/K}$ MEFs was performed on the most frequent tRNA species within this class (right panel). Ratios of intensity values from Northern signals [tRNA fragment vs. mature tRNA] and [tRNA fragment of $Clp1^{K/K}$ MEFs vs. wild type MEFs] are given below. All data have been deposited to GEO (accession number GSE39275).

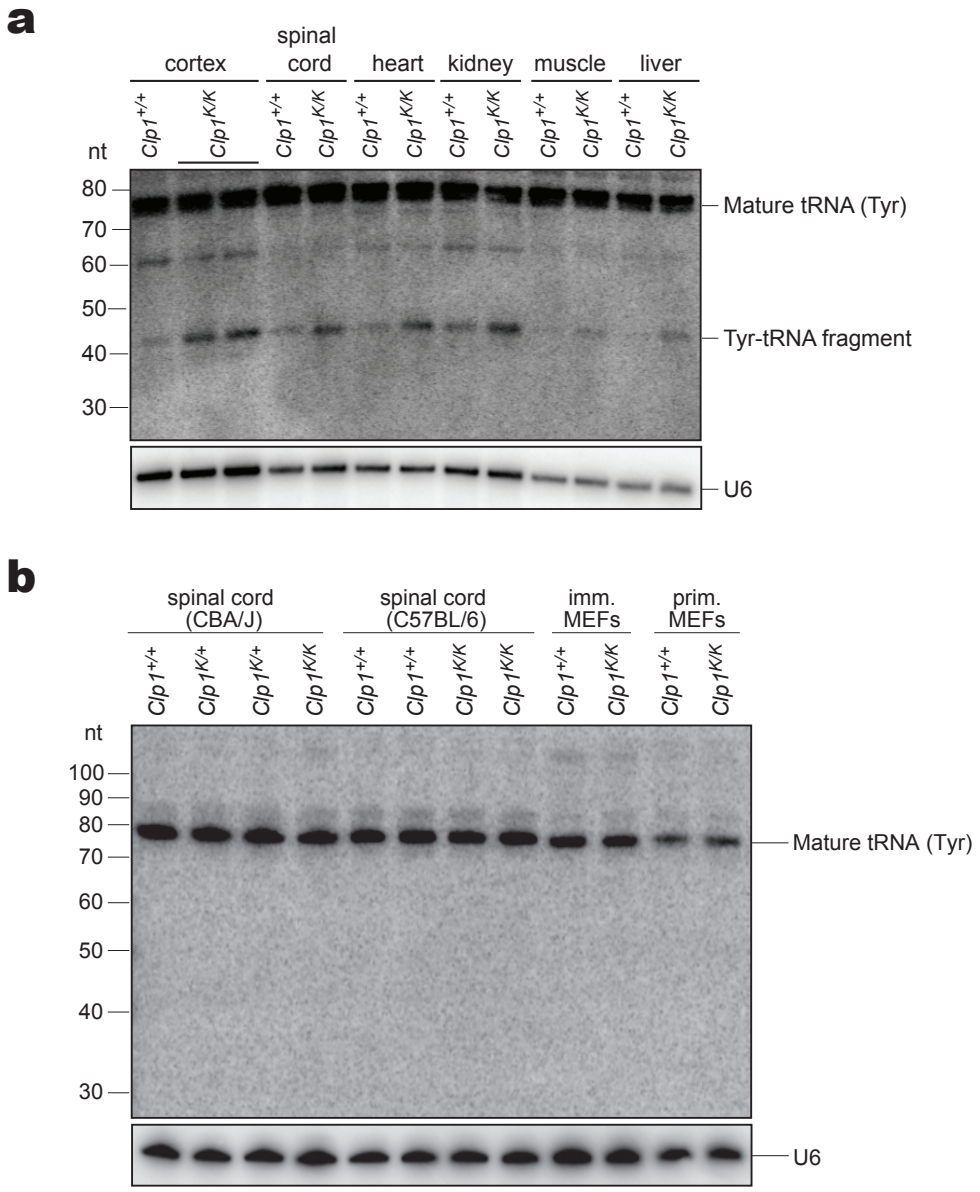

Supplementary Figure 23. Tyrosine tRNA fragments in tissues.

a, Tyrosine tRNA fragments in tissues from control and *Clp1*$^{K/K}$ littermate mice. RNA was isolated from the indicated tissues of 4 months old *Clp1*$^{+/+}$ and *Clp1*$^{K/K}$ mice and analysed by Northern blotting using a probe complementary to the 5' exon region of Tyrosine tRNA. Equal loading of RNA amounts was confirmed by probing for U6 snRNA. **b,** Total RNA was extracted from spinal cord of E18.5 CBA/J and C57BL/6 mice, immortalized and primary MEFs derived from wild type *Clp1*$^{+/+}$, heterozygous *Clp1*$^{K/+}$, and homozygous *Clp1*$^{K/K}$ mice. Northern blotting was performed using a DNA/LNA probe complementary to the 3' exon of tyrosine-tRNAs. Equal loading was confirmed by probing for U6 snRNA.

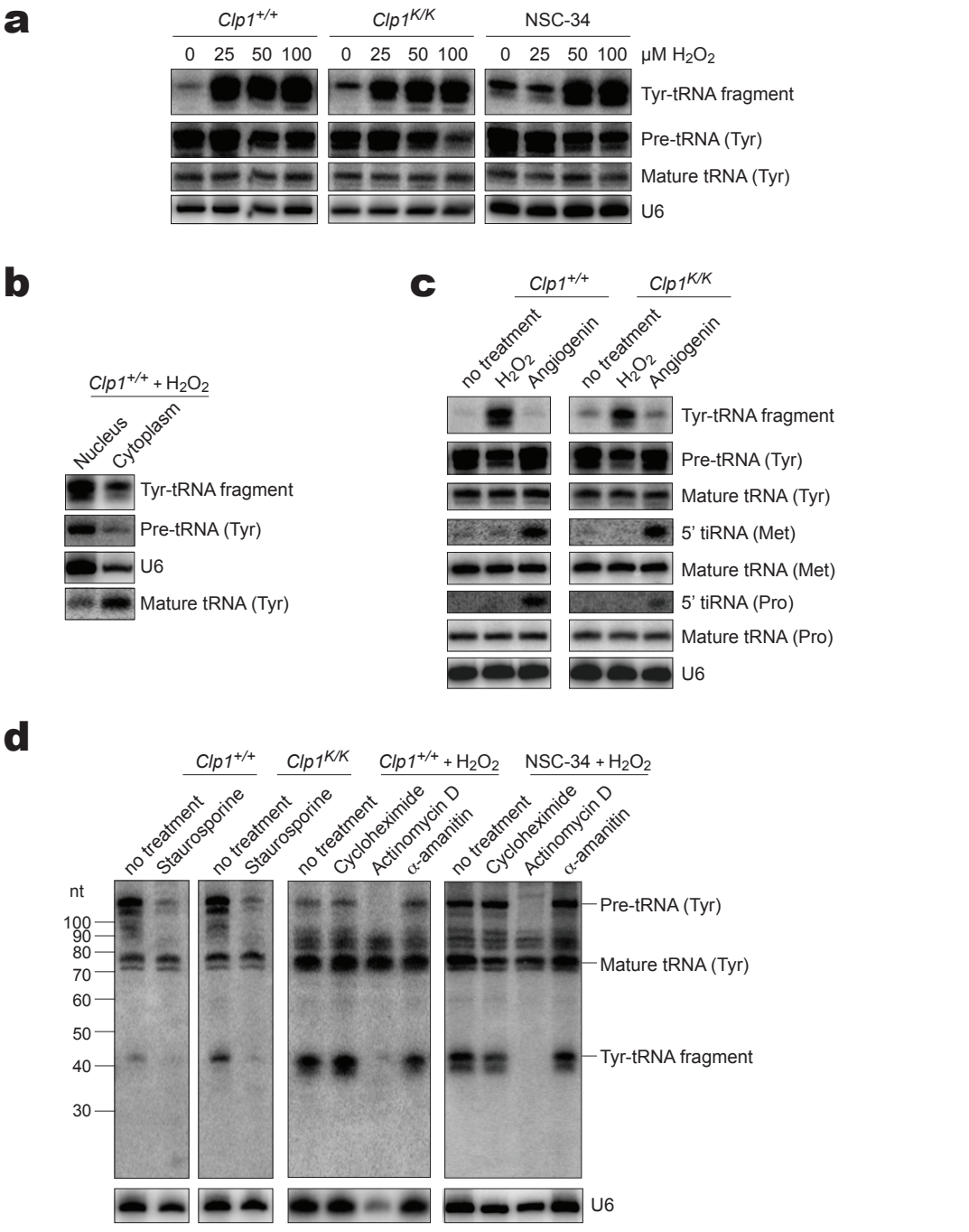

Supplementary Figure 24. Tyrosine tRNA fragments are mainly nuclear and generated from pre-tRNAs by active RNA Pol III transcription.

a, Oxidative stress causes accumulation of Tyr-tRNA fragments. *Clp1*$^{+/+}$ and *Clp1*$^{K/K}$ MEFs and the motor neuron cell line NSC-34 were treated with the indicated concentrations of H_2O_2 for 1 hr. Total RNA was isolated and subjected to Northern analysis. **b,** Tyr-tRNA fragments are mainly nuclear. *Clp1*$^{+/+}$ MEFs were treated with 100 μM H_2O_2 for 1 hr, and cell lysates were fractionated into cytoplasmic and nuclear parts of which RNA was isolated and analysed by Northern blotting. **c,** Generation of Tyr-tRNA fragments is not triggered by Angiogenin. *Clp1*$^{+/+}$ and *Clp1*$^{K/K}$ MEFs were

either left untreated or were treated with 100 μM H_2O_2 or recombinant Angiogenin (1 μg/ml) for 1 hr. RNA was isolated and Northern blot analysis was performed. Note that due to different contrast settings, levels of mature tRNAs (Met; Pro) and 5' tiRNAs (Met; Pro) are not comparable. **d,** Tyr-tRNA fragments are derived from pre-tRNAs and are produced by active RNA Pol III transcription. MEFs or NSC-34 cells (unstressed or stressed by addition of 100 μM H_2O_2 for 1 hr before RNA isolation) were either left untreated or treated with 10 μM of staurosporine for 2 hrs (to induce apoptosis), or for 6 hrs with either 30 μg/ml cycloheximide (to block protein translation), 20 μg/ml actinomycin D (appropriate concentration to block transcription by RNA Pol III in addition to RNA Pol I and II), or 10 μg/ml α-amanitin (to inhibit RNA Pol II transcription). Levels of Tyr-tRNA fragments, but not mature tRNA, are greatly reduced concomitantly with pre-tRNAs when adding staurosporine or actinomycin D to cells, suggesting that active transcription by RNA Pol III is required for the generation of Tyr-tRNA fragments. Levels of Tyr-tRNA fragments remain unchanged after treatment of cells with α-amanitin or cycloheximide, indicating that their generation is not under the control of transcriptional processes by RNA Pol II or protein translation, respectively. Note the decreased levels of U6 snRNA in *Clp1*$^{+/+}$ MEFs due to inhibition of RNA Pol III transcription by actinomycin D.

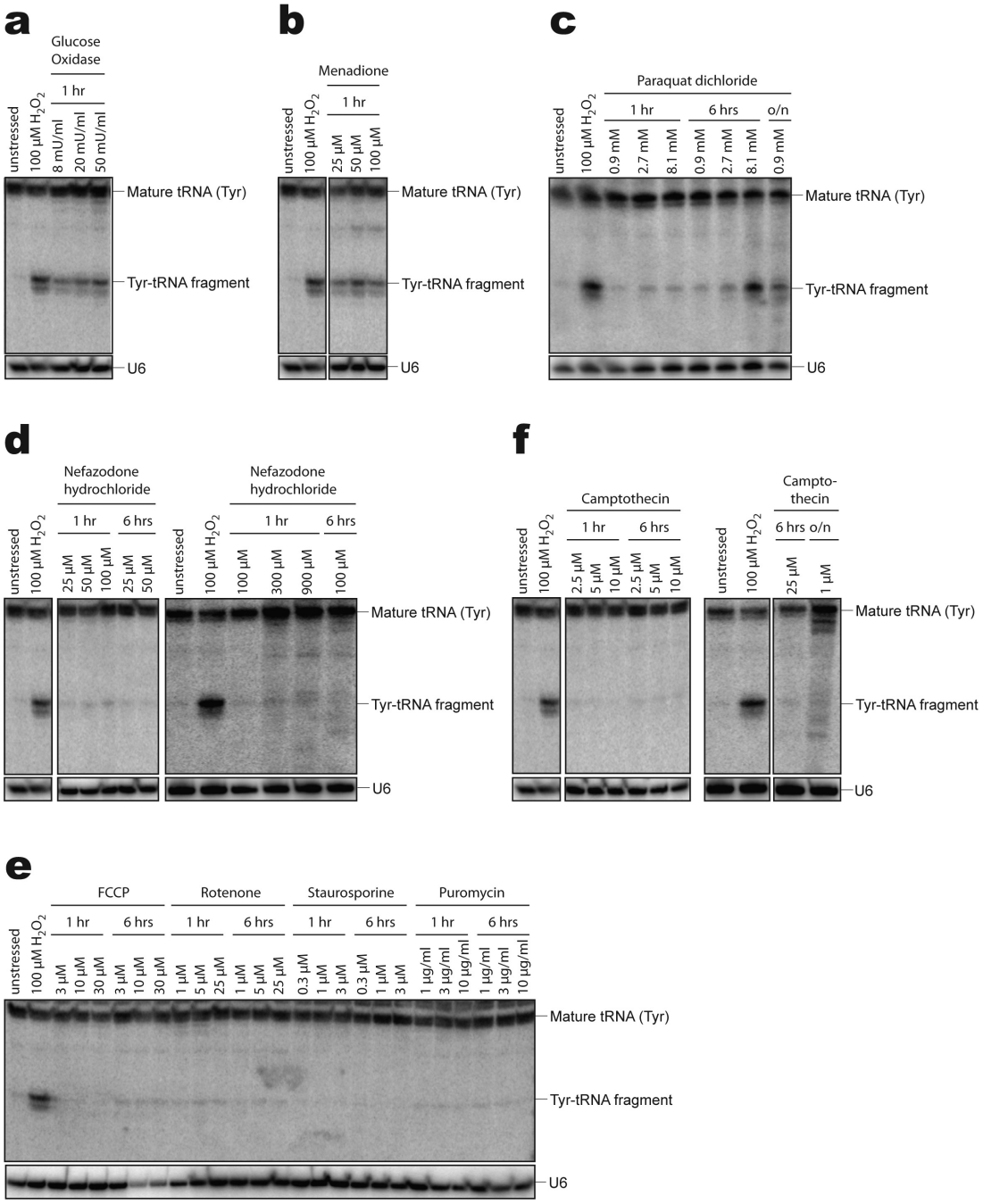

Supplementary Figure 25. Generation of tyrosine tRNA fragments.

Wild-type MEFs were either left untreated or incubated at the indicated concentration and for the indicated time periods with **a,** glucose oxidase, **b,** menadione, **c,** paraquat dichloride, **d,** nefazodone hydrochloride, **e,** the mitochondrial inhibitors FCCP (Carbonyl cyanide 4-(trifluoromethoxy) phenylhydrazone) and rotenone, staurosporine (apoptosis inducer), puromycin (inhibitor of protein translation), and **f**, the DNA damaging agent camptothecin. Tyrosine tRNA fragment generation by cell exposure to H_2O_2 served as positive control. RNA was isolated and analysed by Northern blotting using a probe complementary to the 5' exon region of tyrosine-tRNAs.

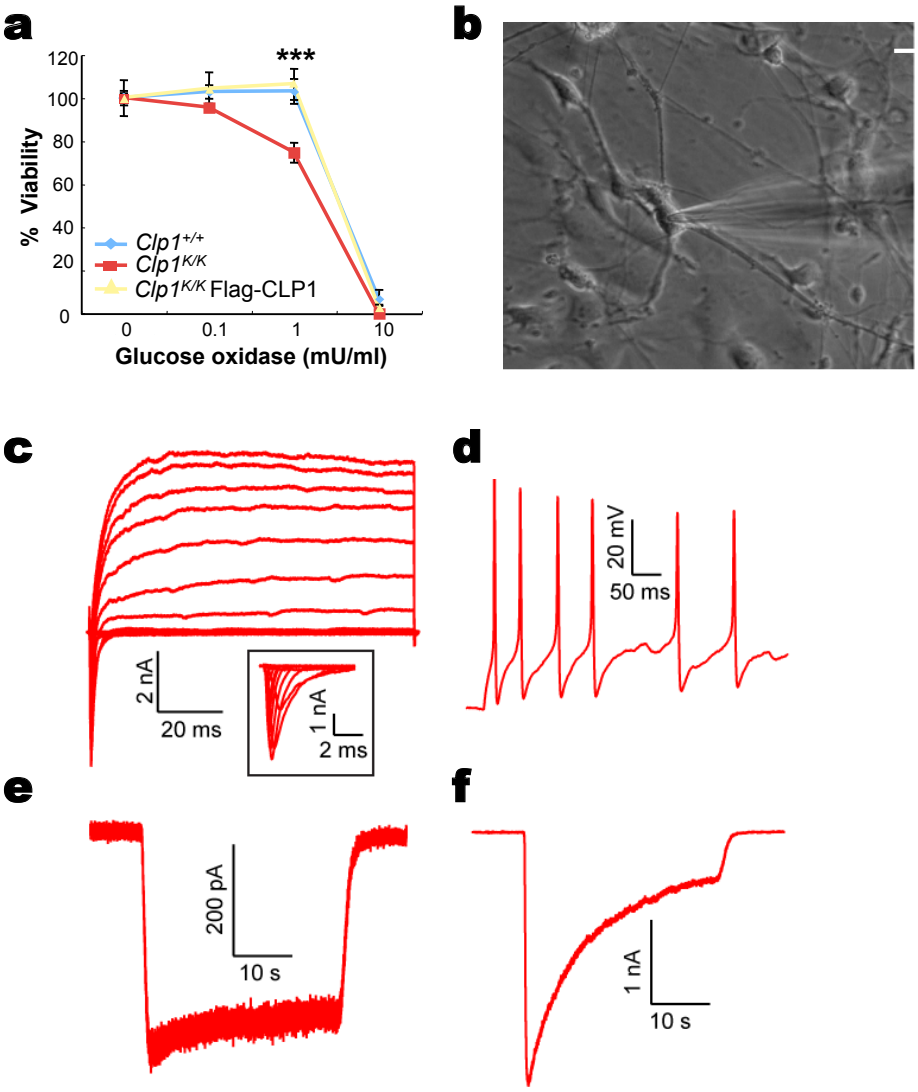

Supplementary Figure 26. Patch clamp analysis of trans-differentiated *Clp1*$^{K/K}$ motor neurons.

a, Viability curves of *Clp1*$^{+/+}$, *Clp1*$^{K/K}$, and *Clp1*$^{K/K}$ 3T3 MEFs rescued with Flag-tagged wild type CLP1. Cells were exposed to the indicated concentrations of glucose oxidase for 20 hours and viability was determined using trypan-blue exclusion. Time point 0 indicates no stimulation. Experiments were performed in triplicate and data are presented as mean values ± S.D. ***$P < 0.001$ (ANOVA). Consistent results were obtained in 3 additional experiments. **b-f,** Patch clamp analysis of trans-differentiated *Clp1*$^{K/K}$ motor neurons. **b,** Bright field image from a Hb9-positive trans-differentiated *Clp1*$^{K/K}$ motor neuron. **c,** Sample voltage clamp recording and inset with blow up of initial sodium current. **d,** Sample current clamp recording. **e,f,** Response to 100 µM kainite **(e)** and 100 µM GABA **(f)**. Of note, the properties of the *Clp1*$^{K/K}$ motor neurons were similar to those of wild type trans-differentiated motor neurons (not shown) and essentially identical to those we have published before[10].

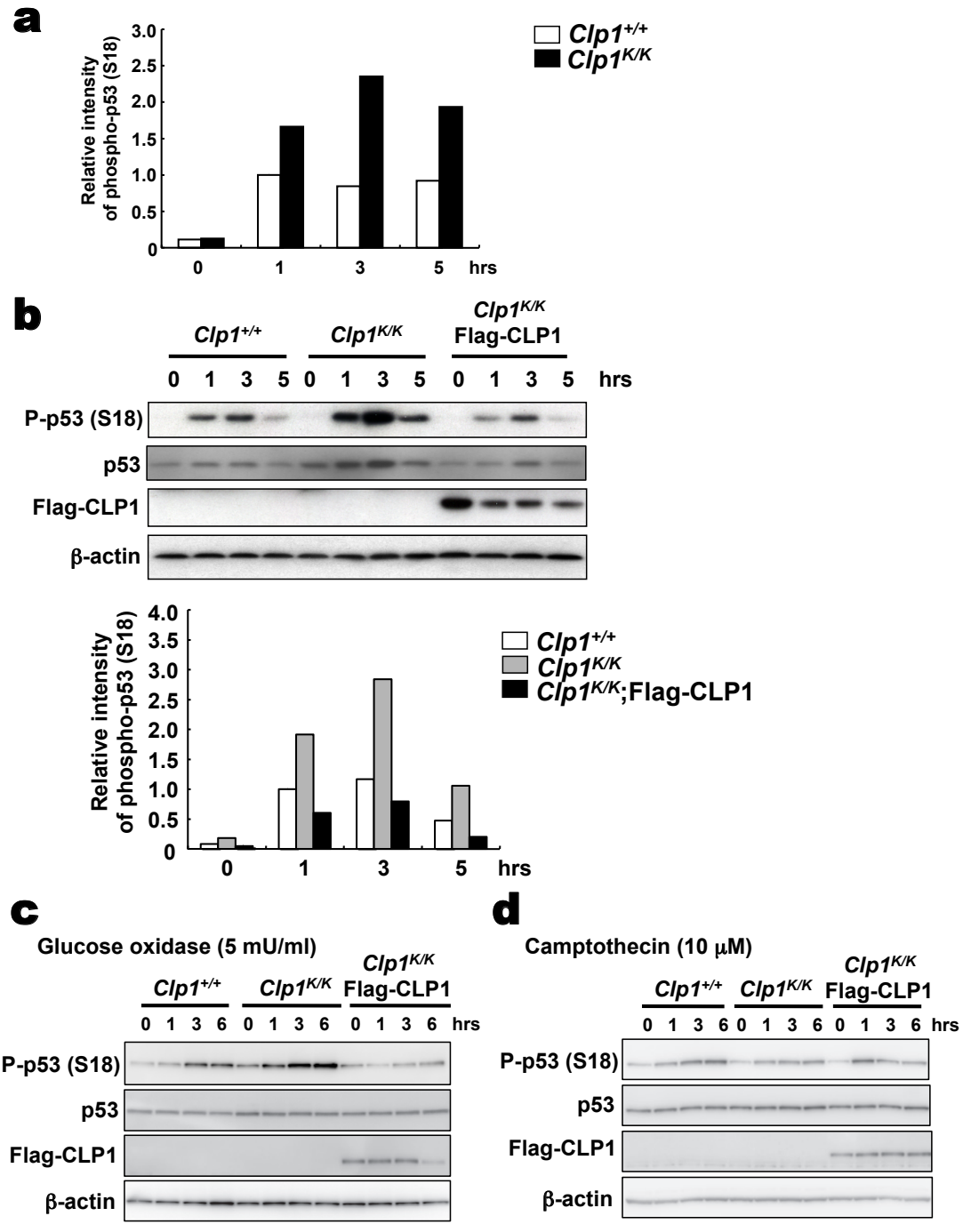

Supplementary Figure 27. Enhanced oxidative stress induced p53 phosphorylation is dependent on CLP1.

a, Quantification of phospho-p53 serine 18 band intensities of H_2O_2 treated (100 μM for 1 hour) *Clp1*$^{K/K}$ primary MEFs as compared to control *Clp1*$^{+/+}$ primary MEFs using semi-quantitative Western blotting. Numbers indicate hours (hrs) of recovery time after stimulation. Time point 0 indicates no stimulation. Quantification of pixel intensity was performed with Metamorph after performing local background subtraction and data was normalized to β-actin loading control. The intensity of normalized phospho-

p53 serine 18 at 1 hour for *Clp1*$^{+/+}$ cells was arbitrarily set at 1.0. Data are represented as mean values of triplicate blots. Similar results were obtained in 3 additional experiments. **b,** Immortalized *Clp1*$^{+/+}$ MEFs, *Clp1*$^{K/K}$ MEFs, and *Clp1*$^{K/K}$ MEFs expressing Flag-tagged CLP1 were exposed to 100 μM H_2O_2 for 1 hour, followed by the indicated recovery time (hours) after exchanging the cell media. Note that the enhanced p53 serine18 phosphorylation in H_2O_2-treated *Clp1*$^{K/K}$ MEFs is rescued by exogenous Flag-CLP1 expression. Total p53 levels and expression of exogenous Flag-CLP1 determined by anti-Flag antibody are shown. β-actin levels serve as loading control. Quantification of phospho-p53 serine 18 band intensities was performed using semi-quantitative Western blotting as above. Data are represented as mean values of triplicate blots. Similar results were obtained in 3 additional experiments. **c,** *Clp1*$^{+/+}$, *Clp1*$^{K/K}$, and *Clp1*$^{K/K}$ 3T3 MEFs expressing Flag-tagged wild type CLP1 were exposed to 5 mU/ml glucose oxidase for indicated times. Time point 0 indicates no stimulation. Note that the enhanced p53 serine18 phosphorylation in glucose oxidase-treated *Clp1*$^{K/K}$ 3T3 MEFs is rescued by exogenous Flag-CLP1 expression. Total p53 levels and exogenous Flag-CLP1 were determined by anti-Flag antibody. β-actin levels served as loading control. Similar results were obtained in 3 additional experiments. **d,** Camptothecin (10 μM) does not trigger enhanced p53 serine 18 phosphorylation in *Clp1*$^{K/K}$ 3T3 MEFs as compared to control MEFs and *Clp1*$^{K/K}$ MEFs expressing Flag-tagged wild type CLP1. Total p53 levels and exogenous Flag-CLP1 were determined by anti-Flag antibody Western blotting. β-actin levels served as loading control. Similar results were obtained in 3 additional experiments.

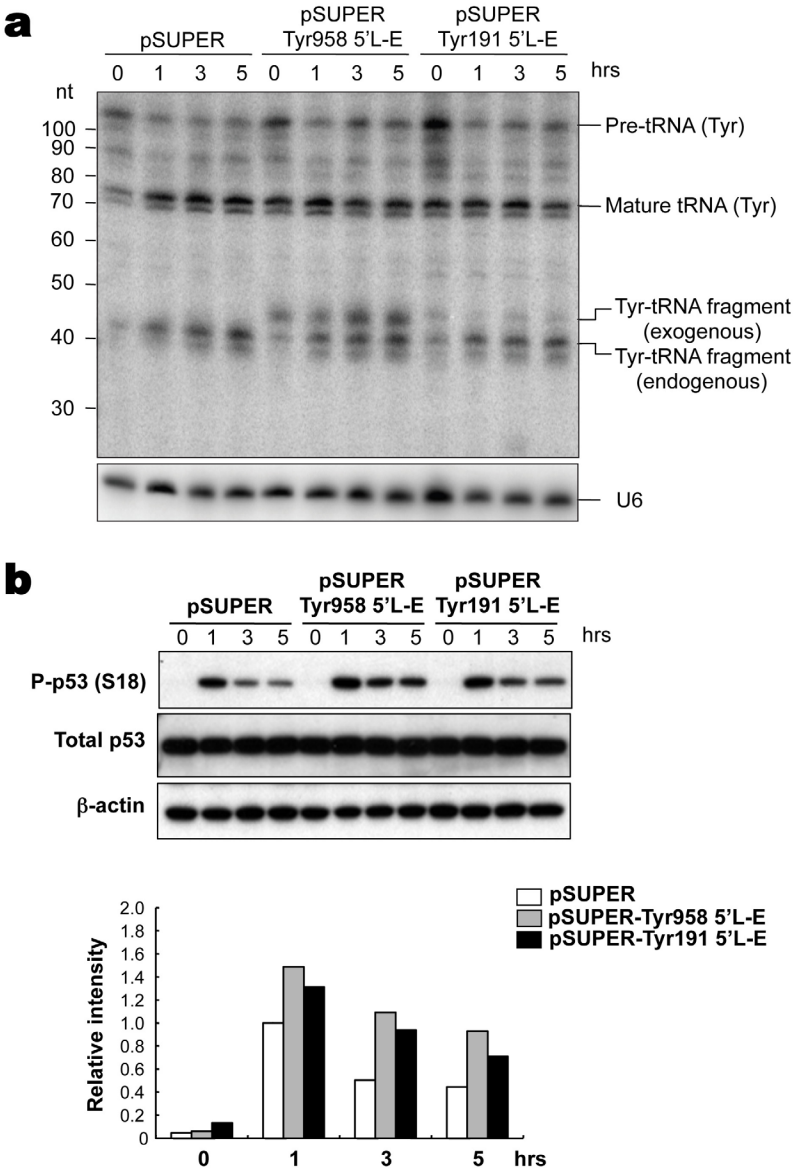

Supplementary Figure 28. Overexpression of Tyr-tRNA fragments in NSC-34 motor neurons augments the p53 phosphorylation after H_2O_2 challenge.

a, Northern blot analysis of the endogenous and exogenously overexpressed Tyr-tRNA fragment in the NSC-34 mouse motor neuron cell line using a DNA/LNA probe complementary to the 5' exon of Tyr-tRNA. Stable cell lines overexpressing the 5' leader-exon (5'L-E) sequences of tRNA191-TyrGTA (pSUPER Tyr191) and tRNA958-TyrGTA (pSUPER Tyr958) fragments were exposed to 50 μM H_2O_2 for 30 minutes, followed by the indicated recovery time (hours) after exchanging the cell media. Note the 2-nt extension of exogenously expressed tRNA fragments as part of the Polymerase III termination site. **b,** Western blot analysis of p53 serine 18 phosphorylation in Tyr-tRNA fragment overexpressing NSC-34 motor neurons. Total p53 levels and β-actin are shown as loading controls. Quantification of phospho-p53 serine 18 band intensities was performed with Metamorph after performing local background subtraction. Data was normalized to the β-actin loading control. The intensity of normalized phospho-p53 serine 18 at 1 hr for the control (empty vector-transfected) cells was arbitrarily set at 1.0. Data are represented as mean values of triplicate blots. Similar results were obtained in 3 additional experiments.

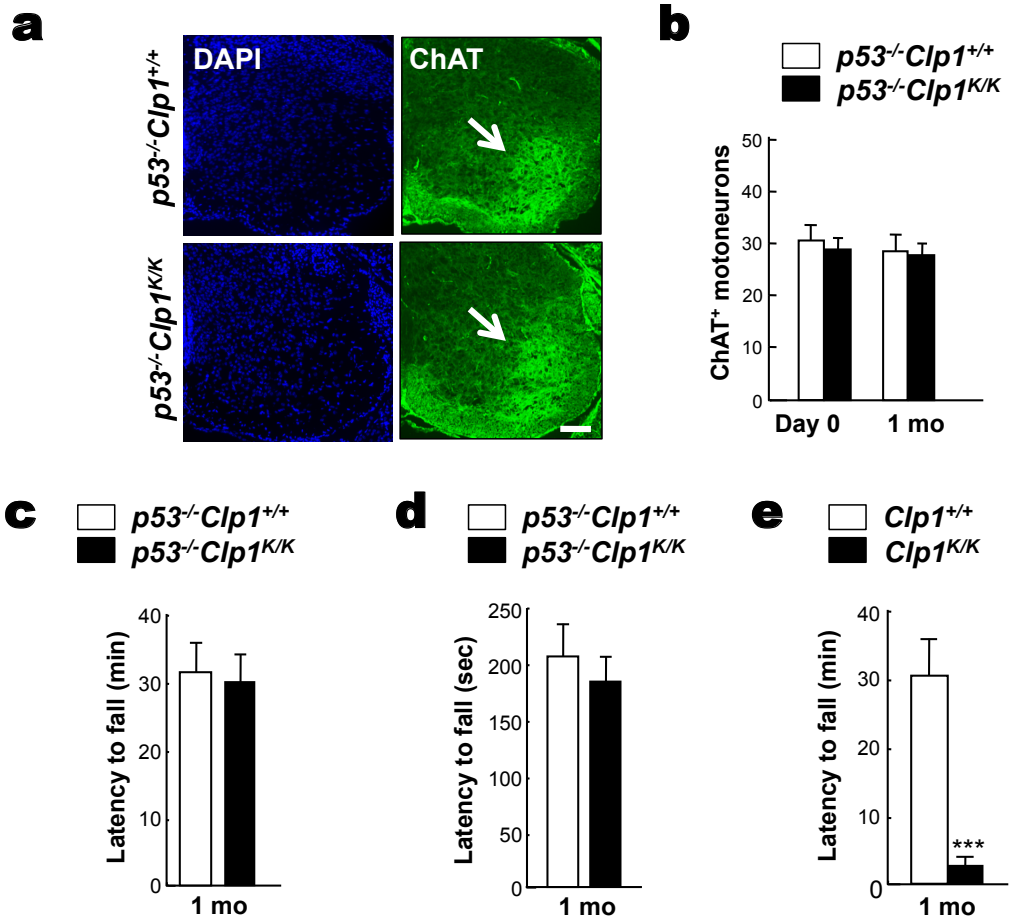

Supplementary Figure 29. Deficiency in p53 rescues the reduced numbers of motor neurons and impaired motor functions of *Clp1*$^{K/K}$ mice.

a, Immunostaining to detect ChAT^{+} (green) motor neurons in the lumbar (L5) spinal cord of newborn p53$^{-/-}$*Clp1*$^{+/+}$ and p53$^{-/-}$*Clp1*$^{K/K}$ littermates on a C57BL/6 background. DAPI staining is shown to visualize nuclei. Scale bar: 50 μm. **b,** Quantification of ChAT^{+} motor neuron numbers in the lumbar (L5) spinal cord of newborn and 1 month (1 mo) old p53$^{-/-}$*Clp1*$^{+/+}$ and p53$^{-/-}$*Clp1*$^{K/K}$ littermates. Data from 5 mice per group presented as mean values ± SD. **c,d,** Normal motor neuron functions in 1 month (1 mo) old p53$^{-/-}$*Clp1*$^{K/K}$ mice as assessed by **c,** the latency to fall in a wire hang assay and **d,** an acceletated Rotarod test. Data are presented as mean values ± S.D. from p53$^{-/-}$*Clp1*$^{+/+}$ (n = 7) and p53$^{-/-}$*Clp1*$^{K/K}$ (n = 4) mice. **e,** Progressive impairment of motor neuron functions in viable *Clp1*$^{K/K}$ mice (on an CBA/J background) as assessed by the latency to fall in wire hang test to demonstrate the rescue in the p53$^{-/-}$*Clp1*$^{K/K}$ mice. Data are from *Clp1*$^{+/+}$ (n = 8) and *Clp1*$^{K/K}$ (n = 7) mice at 1 month, presented as mean values ± S.D. ***P < 0.001 (t-test).

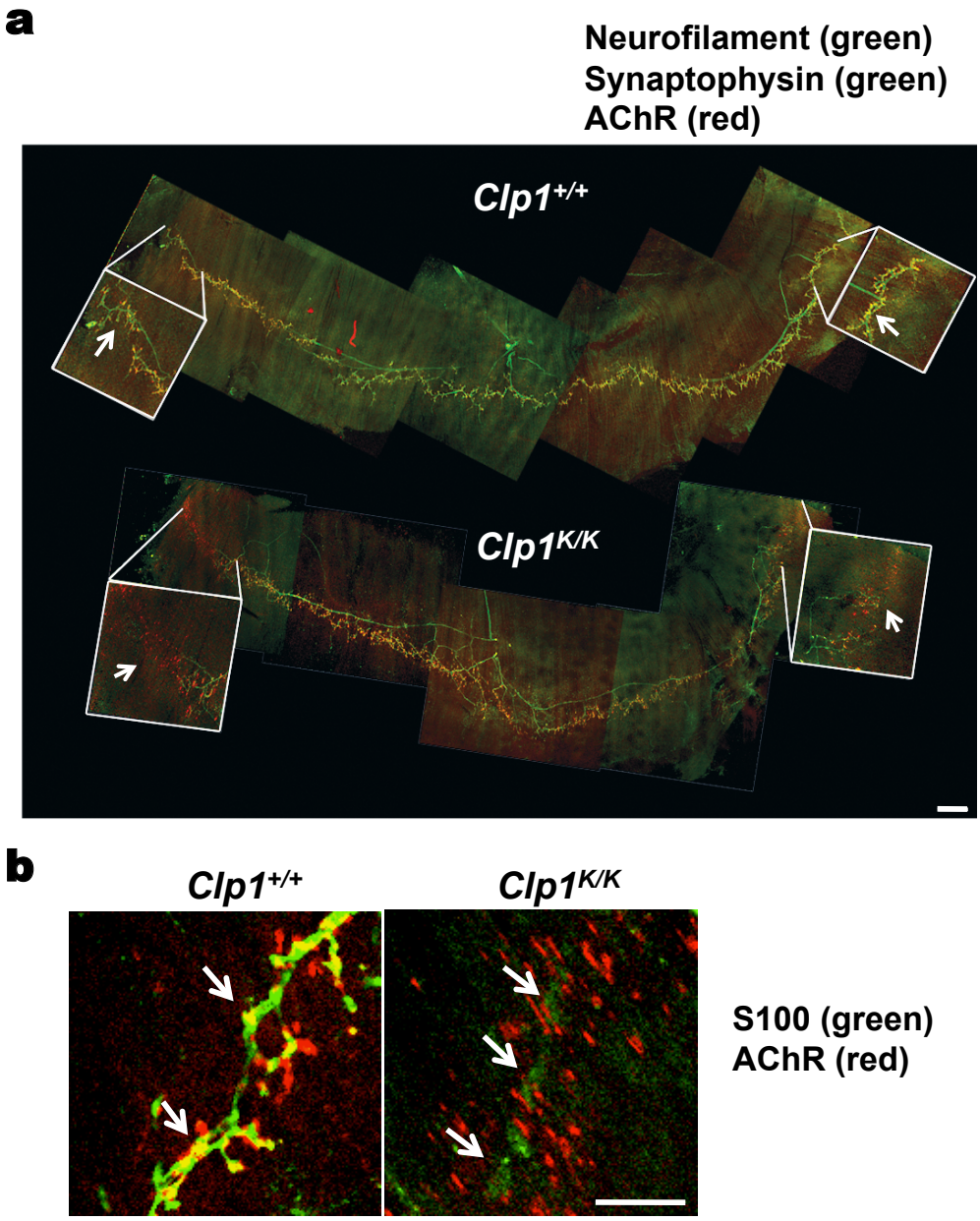

Supplementary Figure 30. Rescue of neonatal lethality of *Clp1*$^{K/K}$ pups by the antioxidant NAC.

a, Whole mount immunostaining of the diaphragm of E18.5 *Clp1*$^{+/+}$ and *Clp1*$^{K/K}$ littermates for postsynaptic acetycholine receptors (AChRs) (red; α-Bungarotoxin) and labeling of the phrenic nerve (green; neurofilament and synaptophysin staining). Pregnant mice were treated with 40 mM of the antioxidant NAC (N-Acetyl-L-cysteine) in the drinking water ad libitum, starting from the day a vaginal plug was found. Water bottles were changed once every three days. Note that denervation in the middle part of the diaphragm of E18.5 *Clp1*$^{K/K}$ embryo was rescued by NAC although the ventral and dorsal tips of the diaphragm were still denervated (arrows). Scale bar: 250 μm. **b,** Whole mount immunostaining of the diaphragm of E18.5 *Clp1*$^{+/+}$ and *Clp1*$^{K/K}$ littermates for acetycholine receptors (AChRs) (red; α-Bungarotoxin) and Schwann cells marked with anti-S100 antibodies (green). The loss of S100 expression (arrows) in the diaphragm of E18.5 *Clp1*$^{K/K}$ embryo is partially rescued by NAC. Scale bar: 100 μm.

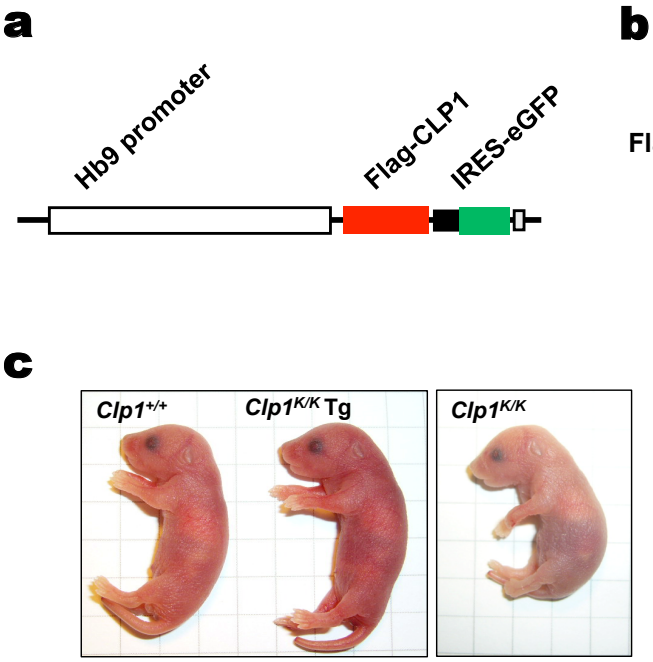

Supplementary Figure 31. Construction of motor neuron specific CLP1 transgenic mice.

a, Schematic representation of the transgenic construct used to re-express wild type CLP1 in motor neurons under the control of the Hb9 promoter. Note that CLP1 is Flag-tagged and the construct also contains an IRES sequence for simultaneous expression of enhanced GFP (eGFP). pA, polyA signal. **b,** Western blot to detect Flag-CLP1 and eGFP expression in spinal cord lysates from two different *Hb9-CLP1* transgenic lines at E14.5. A Non-Tg mouse is shown as control. ***c,*** Appearance of newborn *Clp1*$^{+/+}$ control and *Hb9-CLP1* transgenic *Clp1*$^{K/K}$ (*Clp1*$^{K/K}$ Tg) littermates on a C57BL/6 background. A non-Tg *Clp1*$^{K/K}$ newborn littermate is shown as a control; note the changed skin colour of the pup that died shortly after.

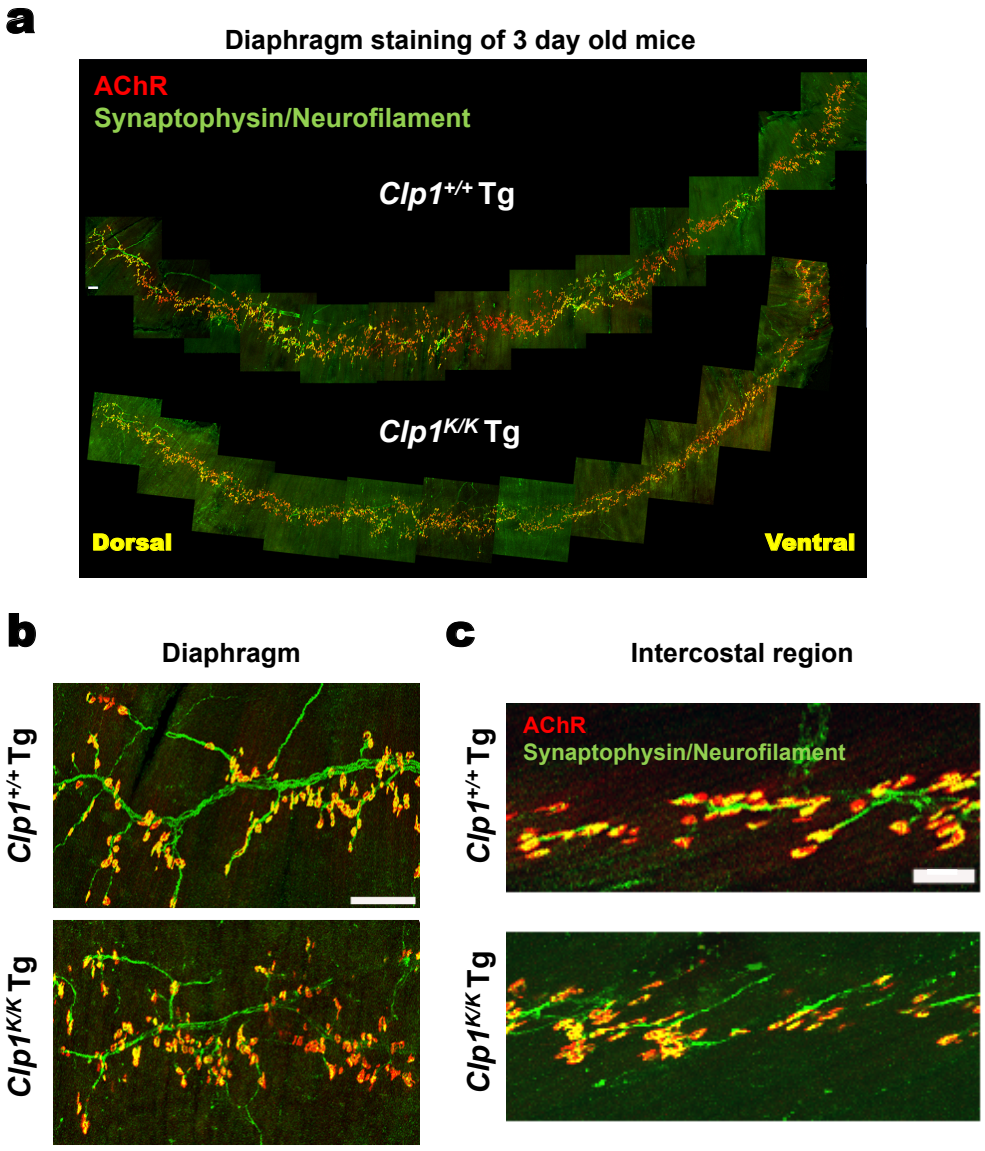

Supplementary Figure 32. CLP1 transgenic expression rescues the motor neuron defects of *Clp1*$^{K/K}$ mice.

a,b, Whole mount immunostaining of the diaphragm of 3 days old *Clp1*$^{+/+}$ Tg and *Clp1*$^{K/K}$ Tg littermates for postsynaptic acetycholine receptors (AChRs) (red; α-Bungarotoxin) and labeling of the phrenic nerve (green; neurofilament and synaptophysin staining). Note the apparently normal NMJ formation, normal fasciculation of the phrenic nerve and normal localization of primary and secondary nerve branches. Scale bars for a and b: 100 μm. **c,** Whole mount immunostaining depicting NMJs in the intercostals region of 3 days old *Clp1*$^{+/+}$ Tg and *Clp1*$^{K/K}$ Tg littermates. Postsynaptic acetylcholine receptor (AChR) clusters (red, stained with α-Bungarotoxin) and innervating motor axons and pre-synaptic nerve terminals (green; double stained with anti-Synaptophysin to visualize NMJs and anti-neurofilament to image axons) are shown. Scale bar: 50 μm.

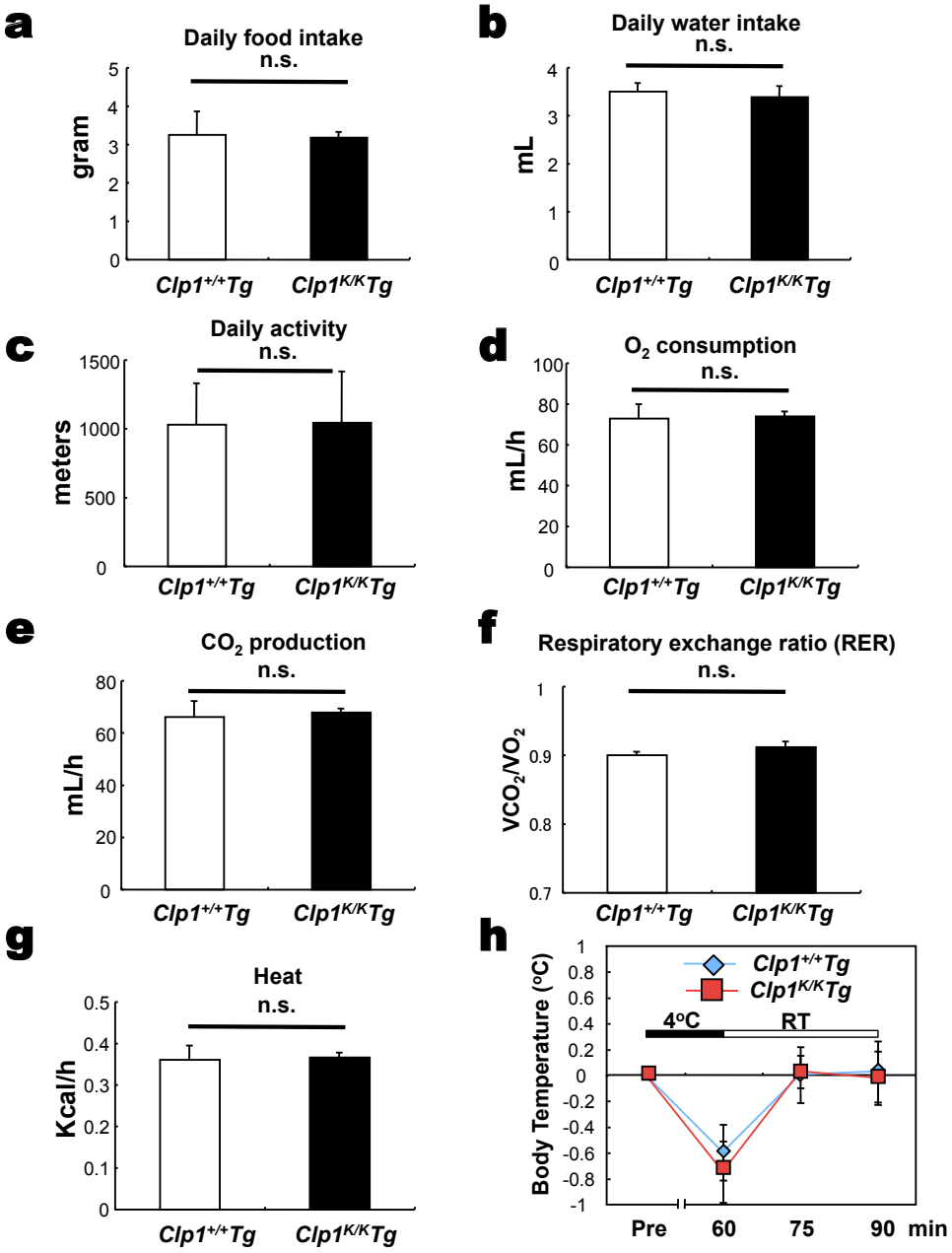

Supplementary Figure 33. Indirect calorimetry and sympathetic nervous system functions in *Clp1*$^{K/K}$ Tg mice.

a, Daily food intake, **b,** daily water intake, **c,** daily activity, **d,** O_2 consumption, **e,** CO_2 production, **f,** respiratory exchange ratio, and **g**, heat production in *Clp1*$^{+/+}$ Tg and *Clp1*$^{K/K}$ Tg littermates. All measurements were performed for 5 consecutive days using an open circuit calorimetry system. **h,** Kinetics of body temperature recovery, as a measure for sympathetic nervous system functions, following cold exposure at 4°C for 1 hour. Rectal body temperatures were measured at 0, 60, 75 and 90 min using a Microprobe thermometer. Data are from 4 mice per group and presented as mean values ± S.E.M. n.s., not significant (t-test).